To the Graduate Council:

I am submitting herewith a thesis written by Vinson B. Huegele entitled "A Study of Some Parameters Affecting Performance of a Laser Vibrometer." I have examined the final copy of this thesis for form and content and recommend that it be accepted in partial fulfillment of the requirements for the degree of Master of Science, with a major in Engineering Science.

W. M. Farmer

W. M. Farmer, Major Professor

We have read this thesis
and recommend its acceptance:

Dennis Keefer

R. A. Beaty

Accepted for the Council:

Carl Minkel

The Graduate School

A STUDY OF SOME PARAMETERS AFFECTING PERFORMANCE OF A LASER VIBROMETER

A Thesis

Presented for the

Master of Science

Degree

The University of Tennessee, Knoxville

Vinson B. Huegele

March 1984

ACKNOWLEDGMENTS

Although many people assisted in this work, the author wishes to recognize certain individuals for special support. Mr. W. H. Goethert initiated and directed the study, and Dr. Bruce W. Bomar gave insight to the electronics and computer related aspects of the work. The author is very much indebted to these men for their help. Also, the author's major professor, Dr. W. M. Farmer, is gratefully acknowledged for his academic supervision and guidance.

The work reported herein was supported by Headquarters, Arnold Engineering Development Center, Arnold Air Force Station, Tennessee, within the terms of Contract F40600-77-C-0003 with ARO, Inc. (renamed Sverdrup Technology, Inc.), under Project P32L-02A. Further reproduction is authorized to satisfy the needs of the U.S. Government.

ABSTRACT

For a laser vibrometer scanning a diffuse surface, the observed signal is dependent partly upon the visibility of the reflected speckle pattern. This study will show that the visibility of the speckle interference fringes is independent of the incident light intensity and dependent on the number of speckle spots. Theoretical aspects of the problem are discussed, and an experimental verification is presented. The results show how signal quality can be improved by using apertures and higher laser powers.

TABLE OF CONTENTS

CHAPTER		PAGE
I.	INTRODUCTION.	1
II.	THEORETICAL CONSIDERATIONS.	4
	Review of Interferometric Principles.	4
	Speckle Pattern and Surface Descriptions. . .	12
	Derivation of a Speckle Mathematical Model	14
	Signal-to-Noise Ratio Definitions and Assumptions	22
III.	EXPERIMENTAL VERIFICATION	25
	Apparatus Description and Operation	25
	Detector Characterization	29
	Aperture Measurements of Visibility and Signal-to-Noise Ratio	35
	Intensity Measurements of Visibility and Signal-to-Noise Ratio	46
IV.	SUMMARY AND CONCLUSIONS	54
BIBLIOGRAPHY.	. . . . .	56
APPENDICES.	. . . . .	58
I.	EVALUATION OF EQUATION (21)	59
II.	COMPUTATION OF IMAGE AND OBJECT RADII	62
VITA.	. . . . .	64

LIST OF FIGURES

FIGURE		PAGE
1.	Example of Signal Dropout.	2
2.	Visibility Definition for a Given Interferometer Irradiance.	11
3.	Geometry Pertinent to Speckle Analysis	16
4.	Optical Arrangement for the Experiment	26
5.	Photograph of the Laser Vibrometer	27
6.	Block Diagram of Optics and Associated Electronics.	30
7.	Beam Profile	32
8.	DC Output versus Incident Irradiance	34
9.	Geometric Optics of Light from Surface to Detector	37
10.	Measured Visibility versus Aperture Area	40
11.	Signal-to-Noise Ratio versus Aperture Diameter	42
12.	Airy Disc Descriptions of Amplitude, Signal-to-Noise Ratio.	43
13.	Visibility versus Detector Output.	47
14.	Signal-to-Noise Ratio versus Detector Output	49
15.	Signals from a Low-Intensity Speckle Pattern.	50

FIGURE PAGE

16. Signals from a High-Intensity Speckle Pattern. 51

17. Signals from a Low-Intensity Speckle Pattern with an Aperture Stop. 52

NOMENCLATURE

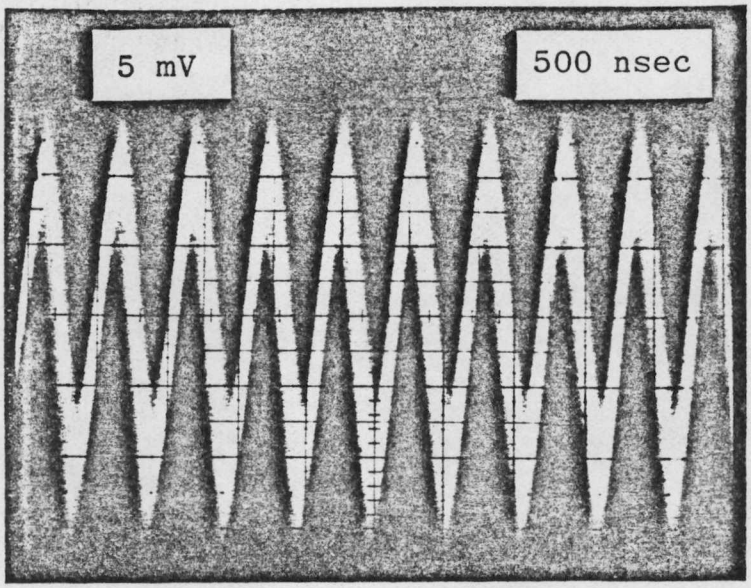
A_s	Spot amplitude
A_1	Field amplitude
A_T	Detector area
a	Source aperture
B	Bandwidth
c	Speed of light
D	Source to image distance
d	Point separation distance
E	Electric field
e	Charge on electron
G	Gain
h	Plane separation distance
I	Intensity
I_p	Photodiode current
J_1	First-order Bessel function
k	Wave number
N	Total noise
N_a	Amplifier noise
N_s	Shot noise
n	Integer speckle spot number
P_a	Average power
P_d	Incident diode power
P_T	Total power
R	Reference beam amplitude

r	Radial variable in focal plane
r_b	Beam radius
r_i	Iris diaphragm radius
r_p	Photometer radius
S	Signal
SNR	Signal-to-noise ratio
T	Argument of cosine
t	Time
V	Voltage
$\bar{v}$	Velocity
v_b	Rate of path length change
x	Path length
z	Load resistance
λ_i	Incident wavelength
λ_r	Reflected wavelength
ϕ	Random phase
ν_i	Incident light frequency
ν_B	Bragg cell frequency
ν_D	Doppler frequency
ν_o	Surface/wavefront intercept rate
ν_S	Frequency shift
θ	Phase term
V	Visibility

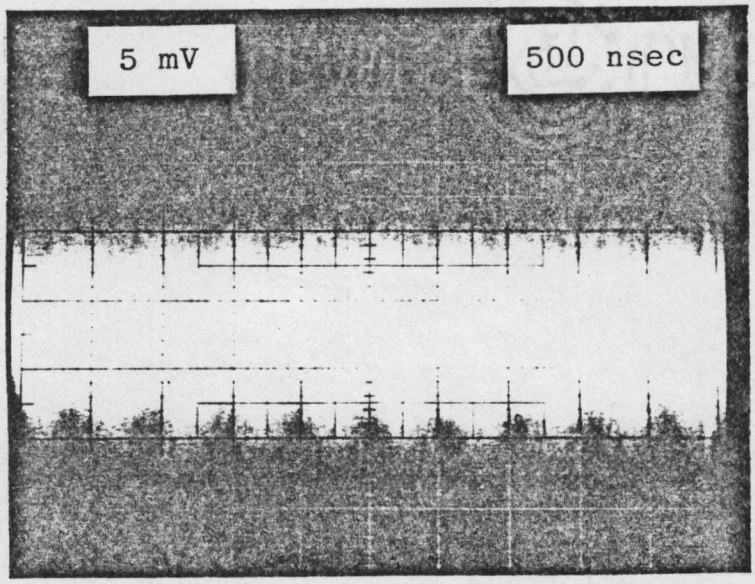
CHAPTER I

INTRODUCTION

The laser vibrometer has been demonstrated as a reliable means for the remote measurement of surface motion. The vibrometer system described in this work uses a laser interferometer with a 10-mW 6328 Å beam modulated at some carrier frequency by Bragg cells. Surface motion in the direction of the impinging beam causes a Doppler shift in the light frequency that is detected by the interferometer and measured in the receiving electronics. When the surface is rough, the reflected laser light is diffusely scattered into random phases so that the resulting signal amplitude is reduced. This scattered light, which generates a speckle pattern, also affects the signal visibility. Since the scattered light is randomly phased, the interference of some speckle patterns can be so poor that the signal amplitude will drop below the noise level. Figure 1 gives an example of such "dropout." At the moment at which there is no signal, the electronics cannot measure surface motion; hence, data are lost. Solutions to reduce the signal degradation of the dropout effect are sought. This investigation will examine some parameters involved.



a. Typical Signal



b. Signal Dropout

Figure 1. Example of Signal Dropout.

The study will generally center around the aspect of signal visibility. The visibility of the fringes in the interferometer is determined by the speckle pattern and other factors. It is measured by the electronics as the ratio of the AC magnitude component to the DC component of the output voltage from the photodiode. It will be shown that, for a specific speckle pattern, different intensities do not alter the visibility within the linearity limits of the photodetector, so that higher powers can be used to obtain a better signal-to-noise ratio (SNR). It will also be shown that the number of speckle spots imaged on the detector affects the visibility. These relationships are developed by a mathematical model representing the speckle pattern as a summation of randomly phased point sources. The model describes the visibility in terms of these parameters and is verified experimentally.

Other factors affecting vibrometer performance including photodetector properties, noise sources, and aperture effects are discussed. These elements are considered theoretically and experimentally as they relate to the problem.

CHAPTER II

THEORETICAL CONSIDERATIONS

Review of Interferometric Principles

The laser vibrometer can be described as a sophisticated version of the Michelson interferometer. Michelson's system splits a single beam into two components of lesser amplitude, so that the system can be considered an amplitude-splitting interferometer [1].[1] The beams are directed along separate paths and recombined to form interference fringes.

If the fields E_1 and E_2 of the split beams are

$$E_1 = A_1 e^{i(2\pi\nu t - k\, x_1)} \tag{1}$$

$$E_2 = A_2 e^{i(2\pi\nu t - k\, x_2)} , \tag{2}$$

where ν is the laser frequency, t is time, k is the wave number, A is the field amplitude, and x is the path length of the respective beams, then the intensity I at the detector plane is

$$I = A_1^2 + A_2^2 + 2\, A_1 A_2 \cos(k(x_1 - x_2)) . \tag{3}$$

---

[1] Numbers in brackets refer to similarly numbered references in the Bibliography.

This expression shows the interference fringes are dependent on the path length difference x_1-x_2. Since a fringe period is defined as a change in optical path by one-half wavelength, the observer can, by measuring the number of fringe displacements, detect small differences in path lengths.

As in the Michelson interferometer, the reference and information beams of the vibrometer are split from a single beam. Both beams enter Bragg cells that shift their frequencies by some ν_B, so that the fields are now

$$E_1 = A_1 e^{i(2\pi(\nu+\nu_{B1})t+k_1x_1)} \tag{4}$$

$$E_2 = A_2 e^{i(2\pi(\nu+\nu_{B2})t+k_2x_2)} . \tag{5}$$

The information beam is directed to the target surface, reflected, and mixed with the reference beam at the beam splitter before entering the photodetector. The intensity of the detector is

$$I = A_1^2 + A_2^2 + 2\, A_1A_2 \cos(2\pi(\nu_{B1}-\nu_{B2})t + (k_1x_1-k_2x_2)) . \tag{6}$$

Because the Bragg shifted frequencies are small relative to the laser frequency, the $(\nu_{B1}-\nu_{B2})$ term corresponds to a beating effect and generates a constant frequency carrier wave.

From here there are several ways to obtain a field expression to describe the change in path length of one beam due to a moving mirror. However, regardless of the analysis, the resulting term is the same.

If x_o is the initial length of the information beam that changes to x_1 in time t, the rate of change v_b is

$$v_b = \frac{x_1-x_o}{t} ,$$

or solving for x_1,

$$x_1 = x_o + v_b t .$$

Multiplying both sides by k_1 gives

$$k_1x_1 = k_1x_o + k_1v_bt . \qquad (7)$$

This v_b is dependent on the mirror solution $\bar{v}$. Since the beam is reflected back on itself, the x_1-x_o corresponds to twice the surface displacement so that $2\bar{v}=v_b$. Substituting into Eq. (4), the field for the information beam is now

$$E_1 = A_1 e^{i(2\pi(\nu+\nu_{B1})t+k_1x_o+k_1 2\bar{v}t)} \quad . \tag{8}$$

The $2\bar{v}k_1t$ term can be developed in another way. The time for the mirror moving at $\bar{v}$ to travel one fringe period $\lambda_1/2$ is

$$t = \frac{\lambda_1}{2\bar{v}} \ ,$$

which corresponds to a frequency of

$$\nu_D = \frac{2\bar{v}}{\lambda_1} \ . \tag{9}$$

This frequency is the value by which the beam frequency is changed due to the moving mirror and is the Doppler shift [2]. The term is analogous to the path length change as well as the frequency shift, as it is seen:

$$2\bar{v}k_1 = 2\bar{v}\,\frac{2\pi}{\lambda_1} = 2\pi\nu_D \ .$$

The Doppler term can be explored even further. The surface is moving at some velocity $\bar{v}$ against the information beam propagating in the direction of unit vector $\hat{e}_i$. The relative velocity between the surface and the wavefronts is $c-(\bar{v}\cdot\hat{e}_i)$, where c is the speed of light, so that the rate ν_o at which the surface intercepts the wavefronts is

$$\nu_o = [c - (v \cdot \hat{e}_i)] \frac{1}{\lambda_i} ,$$

where λ_i is the beam wavelength incident on the surface. To the observer, this frequency shift ν_S is

$$\nu_S = [c - (\bar{v} \cdot \hat{e}_i)] \frac{1}{\lambda_i} + (\bar{v} \cdot \hat{e}_r) \frac{1}{\lambda_r} ,$$

where subscript r refers to reflected components and i to incident. This can be rewritten

$$\nu_S = \nu_i - \frac{\bar{v} \cdot \hat{e}_i}{\lambda_i} + \frac{\bar{v} \cdot \hat{e}_r}{\lambda_r} . \qquad (9a)$$

Since $\nu_r \lambda_r = \nu_i \lambda_i = c$, and the surface motion $V >> c$, then

$$\lambda_r = \frac{\nu_i \lambda_i}{\nu_r} \simeq \lambda_i ,$$

so that Eq. (9a) can be expressed

$$\nu_S = \nu_i + \frac{\bar{v}}{\lambda_i} \cdot (\hat{e}_r - \hat{e}_i) . \qquad (9b)$$

The reflected light along $\hat{e}_r$ is returning along the same path length as $\hat{e}_i$, but in the opposite direction, so that $\hat{e}_r = -\hat{e}_i$ and ν_S is now

$$\nu_S = \nu_i + \frac{\bar{v}}{\lambda_i} \cdot 2\hat{e}_i \ .$$

If the beam is always incident in the direction of the moving surface, then $\bar{v} \cdot 2e_i = 2\bar{v}$, and the frequency of light in the information beam returning from the surface is

$$\nu_S = \nu_i + \frac{2\bar{v}}{\lambda_i} = \nu_i + \nu_D \ .$$

The information beam field can be most simply written

$$E_1 = A_1 e^{i(2\pi(\nu+\nu_{B1}+\nu_D)t+k_1 x_o)} \ , \qquad (10)$$

which is equivalent to Eq. (8). However, using the field in the form of Eq. (8) and mixing it with the reference beam now yields an intensity

$$I = A_1^2 + A_2^2 + 2\, A_1 A_2 \cos(2\pi(\nu_{B1}-\nu_{B2})t + k_1 x_o - k_2 x_2 + 2\bar{v} k_1 t) \ . \qquad (11)$$

This interference equation contains the beat frequency of the carrier wave, a constant arbitrary reference phase contribution, and the Doppler shift.

For a moving source or surface, the beam frequency shifts depending on the direction of the velocity vector $\bar{v}$, so that the direction as well as the magnitude of the

displacement is indicated in the output. In the absence of surface motion ($\bar{v}=o$), a signal is still received, as Eq. (11) shows.

The signal, as will be shown, is dependent upon the fringe visibility. Interference fringes will have this quality of visibility defined by Michelson as

$$V = \frac{I_{max} - I_{min}}{I_{max} + I_{min}} , \tag{12}$$

where I_{max} and I_{min} are the irradiances corresponding to the adjacent maxima and minima in the fringe system. These maxima and minima occur in Eq. (11) when the cosine term is 1 or -1, respectively, giving

$$I_{max} = A_1^2 + A_2^2 + 2\ A_1A_2$$

$$I_{min} = A_1^2 + A_2^2 - 2\ A_1A_2 .$$

Substituting into Eq. (12) and simplifying yields

$$V = \frac{2\ A_1A_2}{A_1^2+A_2^2} . \tag{13}$$

This specifies the amplitude of the interference pattern irradiance relative to the mean value of its irradiance (see Figure 2).

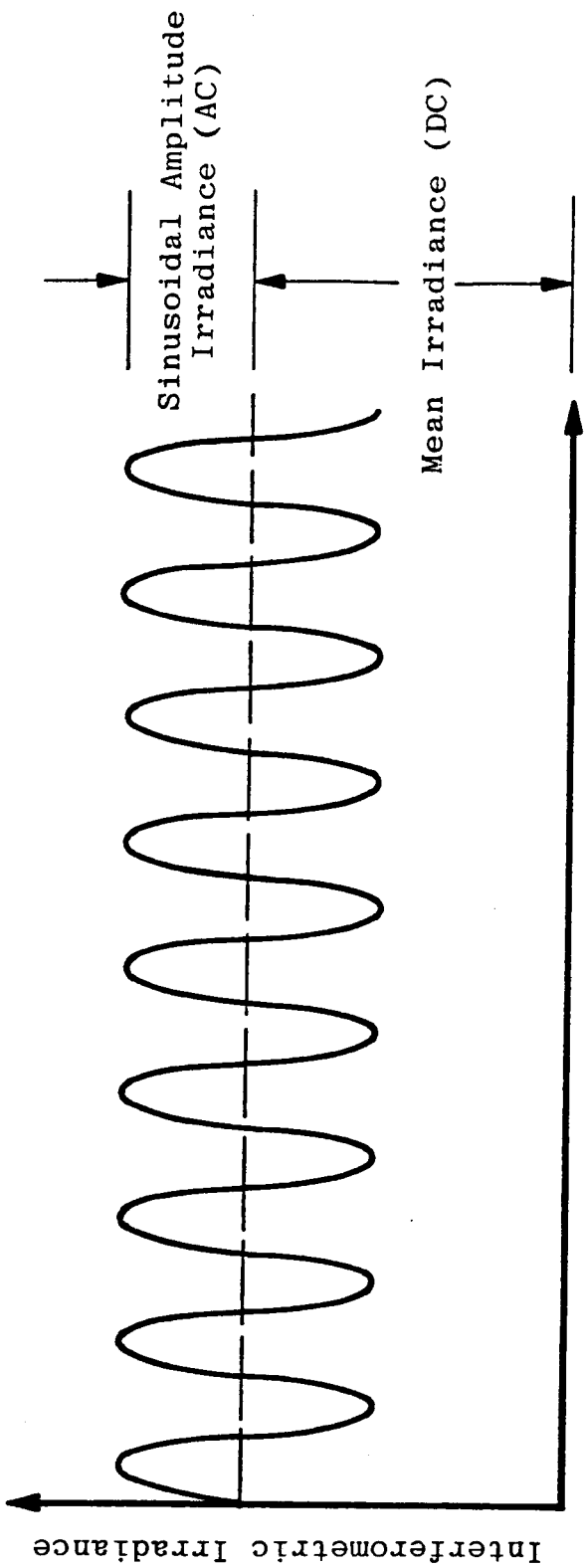


Figure 2. Visibility Definition for a Given Interferometer Irradiance.

The non-varying intensity term $A_1^2+A_2^2$ represents the DC voltage out of the photodetector. The AC signal portion corresponds to the time-dependent cosine term where $2\ A_1A_2$ is the signal amplitude. Visibility can be expressed in terms of detector output by substituting into Eq. (13) to get

$$V = \frac{V_{AC}}{V_{DC}} \ ; \tag{14}$$

V_{AC} and V_{DC} are the respective voltages.

Speckle Pattern and Surface Descriptions

A speckle pattern is essentially an interference phenomenon produced by randomly scattered coherent light, either passing through the atmosphere or reflecting from a diffuse surface. When nearly monochromatic waves are incident on an optically rough surface (i.e., the irregularly arranged surface elements are near in size to the light wavelengths) the reflected light at some far field point consists of many individual wavelets. Each wavelet arises by reflecting from a different microscopic element of the surface and acquires its own random phase. Since the wavelets travel distances differing by several wavelengths, the interference of these wavelets of various phases results in a granular pattern of intensity that is called speckle.

In the case of the laser vibrometer, any rough and unmirrored target that the information beam hits gives rise to speckle. If the vibrating surface were just a plane mirror, the reflection would be of constant phase distribution relative to the incident beam, and signal processing would be much simpler. Speckle, then, in this application, is an unfortunate side effect of the coherent radiation.

The surface used in this study was a tape sprayed with 80 μm spherical glass beads. The tape was applied to the vibrating area being examined. Each bead on the tape acts like a spherical mirror in that it reflects and scatters the light as if it were a point source. Since the beads are randomly arranged on the surface plane, the reflected light generates speckle in the far field.

Within the field in the detector plane will be certain areas of coherent phase. These spots of the speckle occur when the waves from some of the point sources arrive at the detector plane in phase. The entire detector area will receive many speckle spots, each with its own random phase relative to the other, and the output signal is affected. This function of random variables is explained by Goodman [3] as a random walk phenomenon where, instead of n steps, there are n spots. The statistics are the same, as Forrester shows [4], to obtain the root mean

square of the signal from the number of spots. So the number of spots at the detector is now a factor in the signal.

In order to further study the speckle as an interference phenomenon, it is necessary to develop an expression to include all the relationships involved, such as spot number and random phase. A model to describe visibility in these terms will be derived in the next section.

Derivation of a Speckle Mathematical Model

In attempting to describe analytically the speckle pattern, the electromagnetic field of light scattered from a diffuse surface is considered to be produced by an array of random phase point sources in the surface plane. This field is added to a reference beam consisting of planar wave fronts. The intensity of the two interfering beams is calculated for a point in the detector plane a distance, h, away.

Let the diffuse surface be described by an orthogonal grid with phase scatterers centered on the intersections of the grid. The surface is illuminated by a laser source with wavelength, λ, and sufficient beam radius, r_b, to encompass the entire plane under consideration [5]. The field at some (x,y), as shown in

Figure 3, due to a scatterer at (u,v), can be written as

$$E_S = A_1 e^{i(2\pi\nu t - kd + \phi_{uv})} , \qquad (15)$$

where $k=2\pi/\lambda$, d is the distance separating the points, and ϕ is the random phase associated with the specific scatterer at (u,v). Because it is assumed that the separation between scatterers in the plane is small relative to h by, say 1:1,000, some near axis approximations will be made for d using the first terms of the binomial expansion. The distance d can be expressed relative to the position of each point in its respective plane as [6]

$$d = [h^2 + (x-u)^2 + (y-v)^2]^{1/2} .$$

If the scatterers are near the axis so that the detector receives planar waves, that is,

$$(x-u)^2 + (y-v)^2 << h ,$$

then d can be approximated

$$d \approx \left(1 + \frac{(x-u)^2+(y-v)^2}{2h^2}\right)h$$

$$\approx h + \frac{x^2+y^2-2(xu+yv)+u^2+y^2}{2h} + \cdots .$$

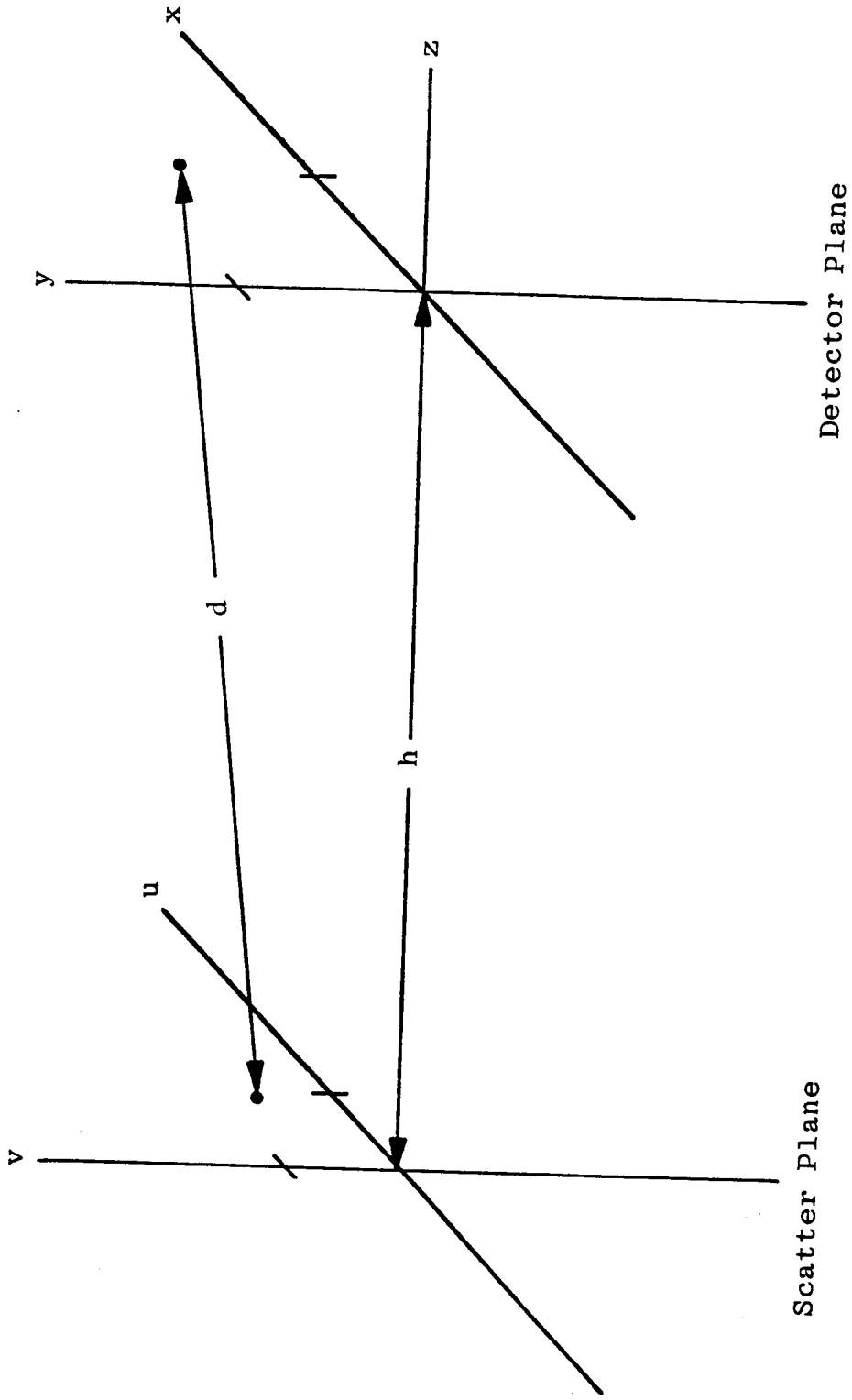


Figure 3. Geometry Pertinent to Speckle Analysis.

The field is then

$$E_S = A_1 e^{i(2\pi\nu t + k(-h-(\frac{x^2+y^2+u^2+v^2-2(ux+vy)}{2h}))+\phi_{uv})} \quad . \qquad (16)$$

The term in the brackets involving $(u^2+v^2)/2h$ is associated only with the scatterer at (u,v) and is a constant value at that point. Since a constant plus a random number is still random, the term is included in ϕ_{uv} without changing the randomness, Eq. (16) is rewritten

$$E_S = A_1 e^{i(2\pi\nu t - kh - \frac{k}{2h}(x^2+y^2) + \frac{k}{h}(ux+vy)+\phi_{uv})} \quad . \qquad (17)$$

The field at (x,y) is the sum of the fields due to all (u,v) from the scatter plane with respective indices j,m.

$$E_{STOT} = \sum_{j=1}^{n} \sum_{m=1}^{n} A_1 e^{i(2\pi\nu t - kh + \frac{k}{h}(u_j x + v_m y)}$$

$$+ \theta + \phi(u_j, v_m) \quad , \qquad (18)$$

letting $\theta = k/2h(x^2+y^2)$.

Now, superimpose a planar reference beam field propagating along the z-axis described by

$$E_R = Re^{i(2\pi\nu_R t - k_R h)} \quad , \qquad (19)$$

where R is the field amplitude and ν_R and k_R are the respective reference frequency and wave number. The resultant field on the detector, provided the fields are still coherent, is

$$E(x,y) = E_R + E_{STOT} \ . \tag{20}$$

The intensity at (x,y) is

$$I(x,y) = E(x,y)\ E^*(x,y)$$

$$= E_R E_R^* + E_{STOT} E_{STOT}^* + 2\ \mathrm{Re}(E_R E_{STOT}^*) \ . \tag{21}$$

A detailed simplification of this equation is given in Appendix I. The results express the intensity as

$$I(x,y) = R^2 + \left[\sum_{j=1}^{n} \sum_{m=1}^{n} A_1 \left(\cos \left(\frac{k}{h}(u_j x + v_m y) + \phi_{(u_j, v_m)} \right) \right) \right]^2$$

$$+ \left[\sum_{j=1}^{n} \sum_{m=1}^{n} A_1 \left(\sin \left(\frac{k}{h}(u_j x + v_m y) + \phi(u_j, v_m) \right) \right) \right]^2$$

$$+ 2R \sum_{j=1}^{n} \sum_{m=1}^{n} A_1 \left(\cos \left(2\pi \Delta\nu (t - \frac{h}{c}) + \theta + \frac{k}{h}(u_j x + v_m y) \right. \right.$$

$$\left. \left. + \phi(u_j, v_m) \right) \right) \ , \tag{22}$$

where $\Delta\nu$ is the difference in information and reference frequencies.

This expression produces with time a maximum and minimum allowing the use of Eq. (12) to determine visibility. By substituting into that visibility formula, the magnitude of the intensity will cancel, leaving the visibility as a function of the speckle pattern and its interference terms and independent of laser intensity.

Although Eq. (22) deals with one point (x,y), the expression is valid when including all (x,y) summed over the detector area. Whether the visibility is for one point or an entire area, the intensity term drops out of Eq. (12). Regardless of laser power, the visibility is seen to be the same, providing the detector response is linear over that power range.

The next investigation is the visibility relation to speckle spot number. Consider the speckle pattern as a region divided into n uniphase regions of equal area. These n spots are small relative to the entire pattern and it is far from the scattering sources so that it is possible to study the spots individually interfering with another wavefront.

Introduce now the reference beam which is the same area as the speckle pattern but sectioned into n regions corresponding to the spots. All portions of the reference beam will have the same phase wavefront, while each speckle spot will have its own random phase. If the

reference segment E_R interferes with a respective speckle spot, the resultant intensity is

$$I = E_R E_R^* + E_{SPOT} E_{SPOT}^* + 2Re(E_R E_{SPOT}^*) \ , \qquad (23)$$

where E_{SPOT} is the field for the spot. This beam of the two interfering fields will generate a signal if received by the detector. The approach is to mix each spot with a reference counterpart for all n regions and evaluate the sum of those contributions that the detector will receive. The intensity of this collection will take the form

$$\begin{aligned} I = {} & E_R E_R^* + E_{SPOT1} E_{SPOT1}^* + 2Re(E_R E_{SPOT1}^*) \\ & + E_R E_R^* + E_{SPOT2} E_{SPOT2}^* + 2Re(E_R E_{SPOT2}^*) \\ & + \cdots \\ & \vdots \\ & + E_R E_R^* + E_{SPOTn} E_{SPOTn}^* + 2Re(E_R E_{SPOTn}^*) \ . \end{aligned}$$

Switching to summation notation,

$$\begin{aligned} I &= nE_R E_R^* + \sum_{j=1}^{n} E_{SPOTj} E_{SPOTj}^* + \sum_{j=1}^{n} 2Re(E_R E_{SPOTj}^*) \\ &= n|E_R|^2 + \sum_{j=1}^{n} |E_{SPOTj}|^2 + 2Re\left(\sum_{j=1}^{n} E_R E_{SPOTj}^* \right) . \qquad (24) \end{aligned}$$

In the previous section it was mentioned that the random phased spots combine in a random walk fashion at the detector [3,4]. The Gaussian statistics of the problem show the resultant collection of spot amplitudes in the entire speckle field amplitude A_l to be

$$A_l = \sqrt{n}\, A_s \ ,$$

where A_s is the individual mean spot amplitude. Applying this to the form in the above summation yields

$$\sum_{j=1}^{n} E_{SPOTj} = \sqrt{n}\, E_{SPOT} \ . \tag{25}$$

Substituting this in, Eq. (24) can now be written

$$I = n|E_R|^2 + (\sqrt{n}|E_{SPOT}|)^2 + 2Re(E_R\sqrt{n}\, E_{SPOT}^*) \ . \tag{26}$$

From Eqs. (12) and (13) the visibility of the irradiance is

$$V = \frac{2|E_R\sqrt{n}\, E_{SPOT}|}{n|E_R|^2+n|E_{SPOT}|^2} = \frac{1}{\sqrt{n}} \frac{2|E_R E_{SPOT}|}{|E_R|^2+|E_{SPOT}|^2} \ . \tag{27}$$

Finally, assume the total amplitudes of each beam are equal for optimum heterodyning; that is, $|E_R|=|E_{SPOT}|$, rendering the visibility

$$V = \frac{1}{\sqrt{n}} \ . \tag{28}$$

This is the relationship between the visibility and the number of spots in the speckle pattern.

Signal-to-Noise Ratio Definitions and Assumptions

Because this study deals with signals from stationary surfaces, complicated signal processing systems and electronics usually employed to monitor vibrational modes are not needed. It is the quality of the signal that is being examined and not necessarily the information it carries. This signal quality is generally expressed in a signal-to-noise ratio (SNR). To describe the SNR, the noise sources of the system are considered.

The photodetector used in the system, an avalanche photodiode with internal amplifier, is assumed to have only two significant noise sources: amplifier noise and shot noise. Shot noise, N_s, is the greater source and, for the non-saturation region of the photodiode, is expressed by the Schottky shot noise formula [7]

$$N_s = Gz\sqrt{2eBI_p}\,, \tag{29}$$

where G is the detector current gain, z is the load resistance, B is the bandwidth, and e is the charge on an electron. The photodiode current I_p, in terms of the DC voltage V_{DC}, is

$$I_p = \frac{V_{DC}}{zG} \quad . \tag{30}$$

To get the noise expression in terms of V_{DC}, Eq. (30) is substituted into Eq. (29) to obtain

$$N_s = Gz \sqrt{2eB \frac{V_{DC}}{Gz}} \quad . \tag{31}$$

The other source, the photodiode, will contribute a small amount of noise, N_a, due to dark current.

The total noise for two uncorrelated sources is

$$N = \sqrt{N_a^2 + N_s^2} \quad . \tag{32}$$

The signal, S, will be considered as the AC portion of the detector output voltage

$$S = V_{AC} \quad . \tag{33}$$

This output is channeled through a low-pass filter. Since the signal frequency from the heterodyning is 2 MHz, the filter eliminates any higher frequencies that would increase the noise level. An oscilloscope receives and displays the signal.

To get the signal-to-noise ratio voltage expression, Eq. (33) is divided by Eq. (32) and substitution of Eq. (31) to get

$$SNR = \frac{V_{AC}}{\sqrt{N_a^2 + \left(Gz \sqrt{2eB \frac{V_{DC}}{Gz}}\right)^2}} . \qquad (34a)$$

The SNR is now given in terms of the primary measurable variables V_{AC} and V_{DC}.

To see the relationship between SNR and visibility, Eq. (14) is solved for V_{DC} and substituted into Eq. (34) to get

$$SNR = \frac{V_{AC}}{\sqrt{N_a^2 + \left(Gz \sqrt{\frac{2eB}{Gz} \frac{V_{AC}}{V}}\right)^2}} . \qquad (34b)$$

CHAPTER III

EXPERIMENTAL VERIFICATION

Apparatus Description and Operation

The operation of the vibrometer can be best understood by tracing the beam path as it leaves the laser (Figures 4 and 5 illustrate the optical arrangement). The beam enters the first Bragg cell which is used as a variable beam attenuator. It is driven at its own optimum frequency that is unrelated to the rest of the system. The second Bragg serves two purposes. It acts as a beam splitter to separate the initial beam into the reference and information beams, and it modulates the deflected reference beam at a Bragg frequency of 36 MHz. The undeflected information beam enters the third cell and is shifted a frequency of 34 MHz (2 MHz different than the reference beam). It is this 2 MHz that becomes the carrier wave and is displayed as the signal. The information beam then passes through a Wollaston prism and quarter-wave plate to the surface.

The Wollaston prism/quarter-wave unit and polarizing effects are introduced to provide a convenient, efficient way of separating the incoming information beam from the reflected scattered light. Rather than

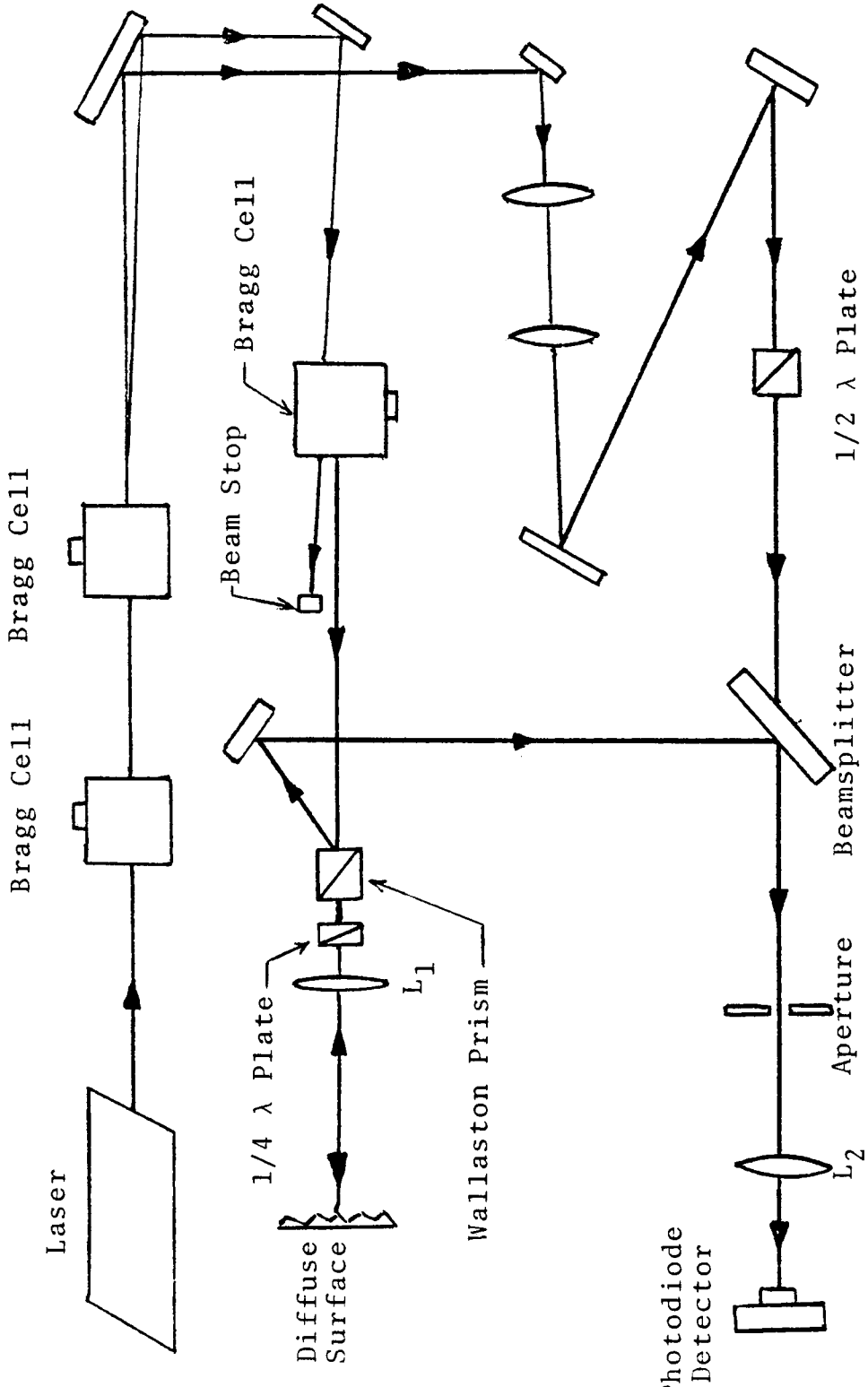


Figure 4. Optical Arrangement for the Experiment.

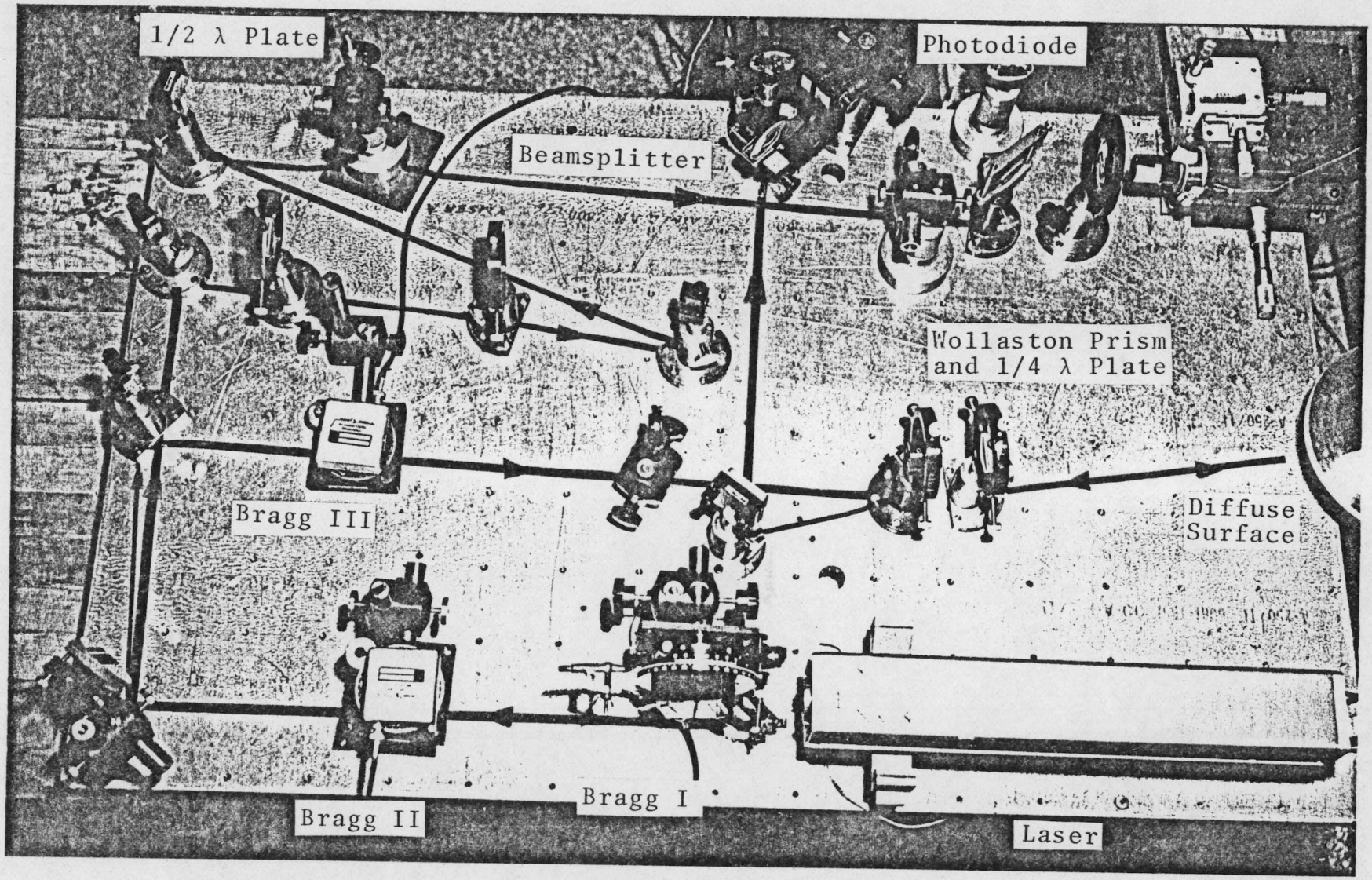


Figure 5. Photograph of the Laser Vibrometer.

incorporate a partially silvered mirror that would greatly reduce the beam intensity, the prism unit allows beam separation with less intensity reduction.

The Wollaston prism permits a vertically polarized beam, such as the laser output, to travel a different path than that of a horizontally polarized beam. In the vibrometer system, the beam enters the prism and then the quarter-wave plate which changes the polarization from linear to circular. A lens (L_1) focuses on the laser energy on the surface as well as collects the scattered light. As the light returns from the test surface, the second pass through the quarter-wave plate changes the polarization from circular back to linear as well as rotating the polarization vector 90^o relative to the original beam. The prism deflects this rotated beam away from the axis of the incoming information beam, neatly separating the two. The scattered light and its associated speckle pattern is mixed with the reference beam at the beam splitter. To provide for path length matching and wavefront alignment for optimum optical heterodyning, appropriate lenses and mirrors were added in the reference beam. Also, a half-wave plate was inserted to match the polarization incurred in the information beam by the Wollaston/quarter-wave unit. Finally, the combined beams

are focused by lens L_2 on the photodetector. A block diagram of the optics and associated electronics is shown in Figure 6.

The detector used was an RCA C30818 DC coupled avalanche photodiode with internal amplifier. A DC coupled unit was chosen so that a DC voltage output level, as well as the AC amplitude of the signal, would be available for the visibility and SNR calculations. Also, this detector was selected because of its high responsivity to the laser wave length and associated light intensities.

Detector Characterization

Since the study assumes the detector will have a linear response, it is necessary to know the range of that response. To find this range, the incident light power on the detector must be measured. But because of the small area of the photodiode relative to the full beam, the incident power is not easily measured directly. The measurement can be made indirectly with a photometer.

A photometer measures the incident light power over the area of its detector. This averaged power, P_A (for a Gaussian intensity distribution), is

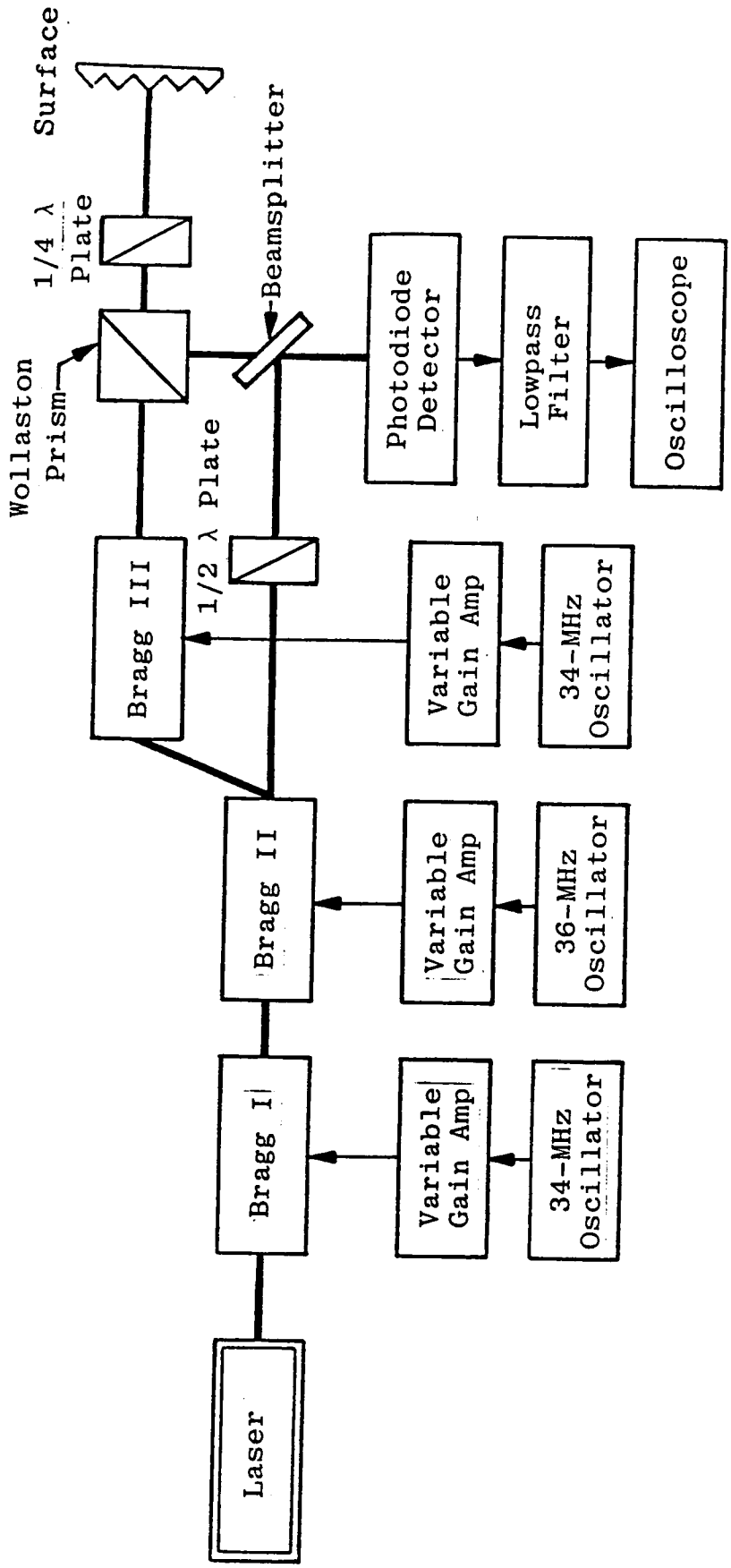


Figure 6. Block Diagram of Optics and Associated Electronics.

$$P_A = P_T\left(1 - e^{-2\left(\frac{r_p}{r_b}\right)^2}\right), \qquad (35)$$

where P_T is the total power within the beam radius, r_b, and $r_p > r_b$ is the photometer sensor radius [8]. Similarly, the diode incident power, P_d, will be

$$P_d = P_T\left(1 - e^{-2\left(\frac{r_d}{r_b}\right)^2}\right), \qquad (36)$$

where r_d is the radius of the photodiode surface.

To measure r_b, the photometer was masked with an 800-μm aperture and scanned across the center of the aperture and scanned across the center of the beam at the detector plane. Since the beam appeared to be about a half-inch wide, the aperture was assumed small enough to plot an accurate beam profile. The beam diameter was found from the intensity versus position plot in Figure 7.

Now, knowing r_d, and substituting Eq. (35) into Eq. (36),

$$P_d = \frac{P_A\left(1 - e^{-2\left(\frac{r_d}{r_b}\right)^2}\right)}{\left(1 - e^{-2\left(\frac{r_p}{r_b}\right)^2}\right)} \qquad (37)$$

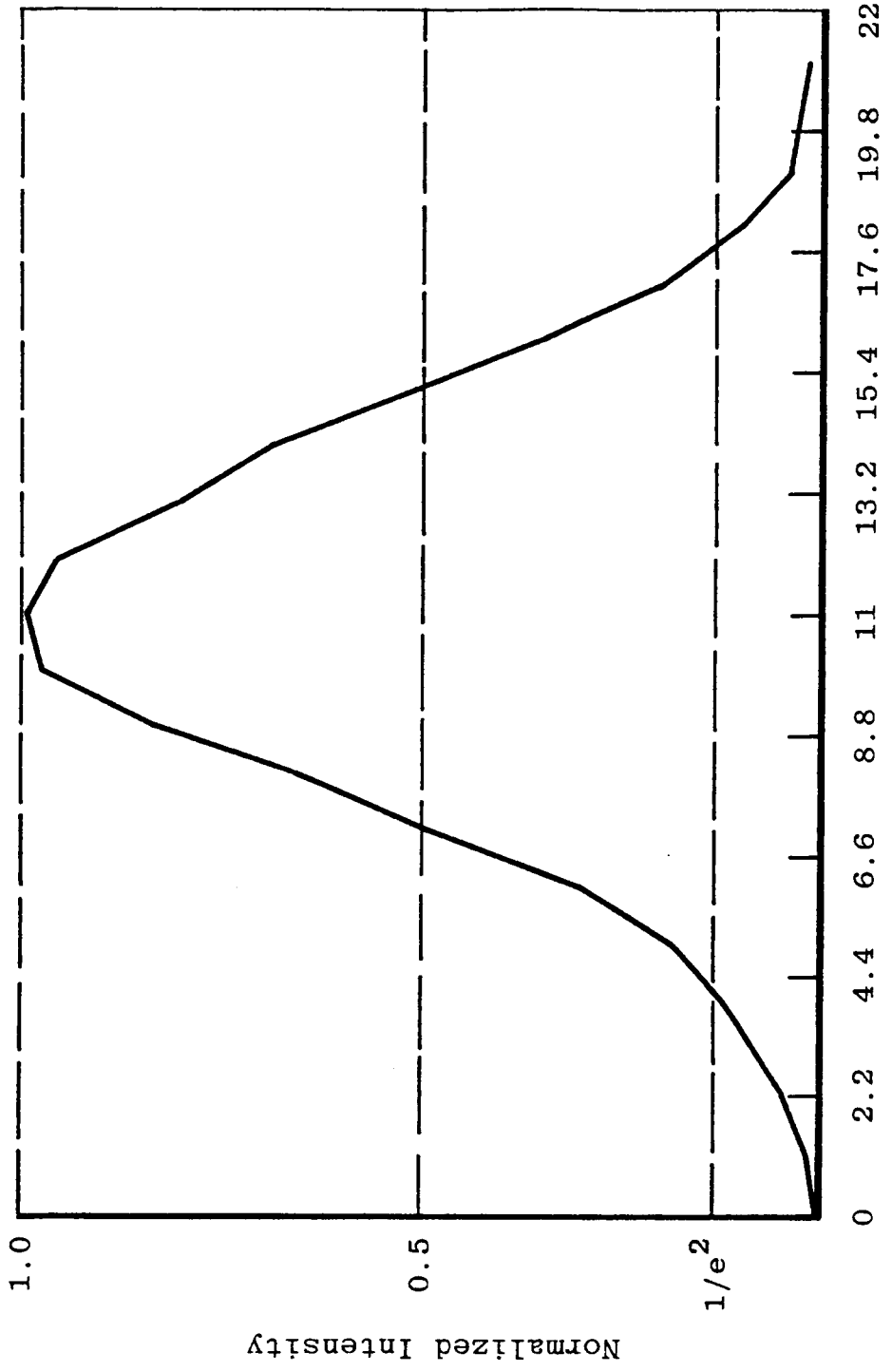


Figure 7. Beam Profile.

gives the light power on the diode by measuring the entire beam power with the photometer.

The next step in characterizing the photodiode detector involves determining the fraction of the incident beam deflected by a Bragg cell as a function of the input power to the cell. To find this relationship, the deflected first-order beam from a cell was directed into the photometer. The input to the Bragg cell was controlled by a frequency generator which regulated both frequency and voltage amplitude of the signal. For a constant frequency (here, 15 MHz), the Bragg input power was incremented by varying the driver amplitude in 5-mV units. The resulting deflected light to the photometer was measured. With these data, it was possible to determine the first-order diffracted beam power by measuring the input signal to the Bragg cell.

Replacing the photometer with the photodiode provided the correlation between Bragg diffracted light power and diode current by varying the driven amplitude and measuring the resulting detector output current. With these measurements, the diode voltage can be plotted against the incident power to determine the linear range of the detector. This plot is shown in Figure 8. The diode was found to saturate around 5-μW incident power or about 800-mV DC output. The average measured

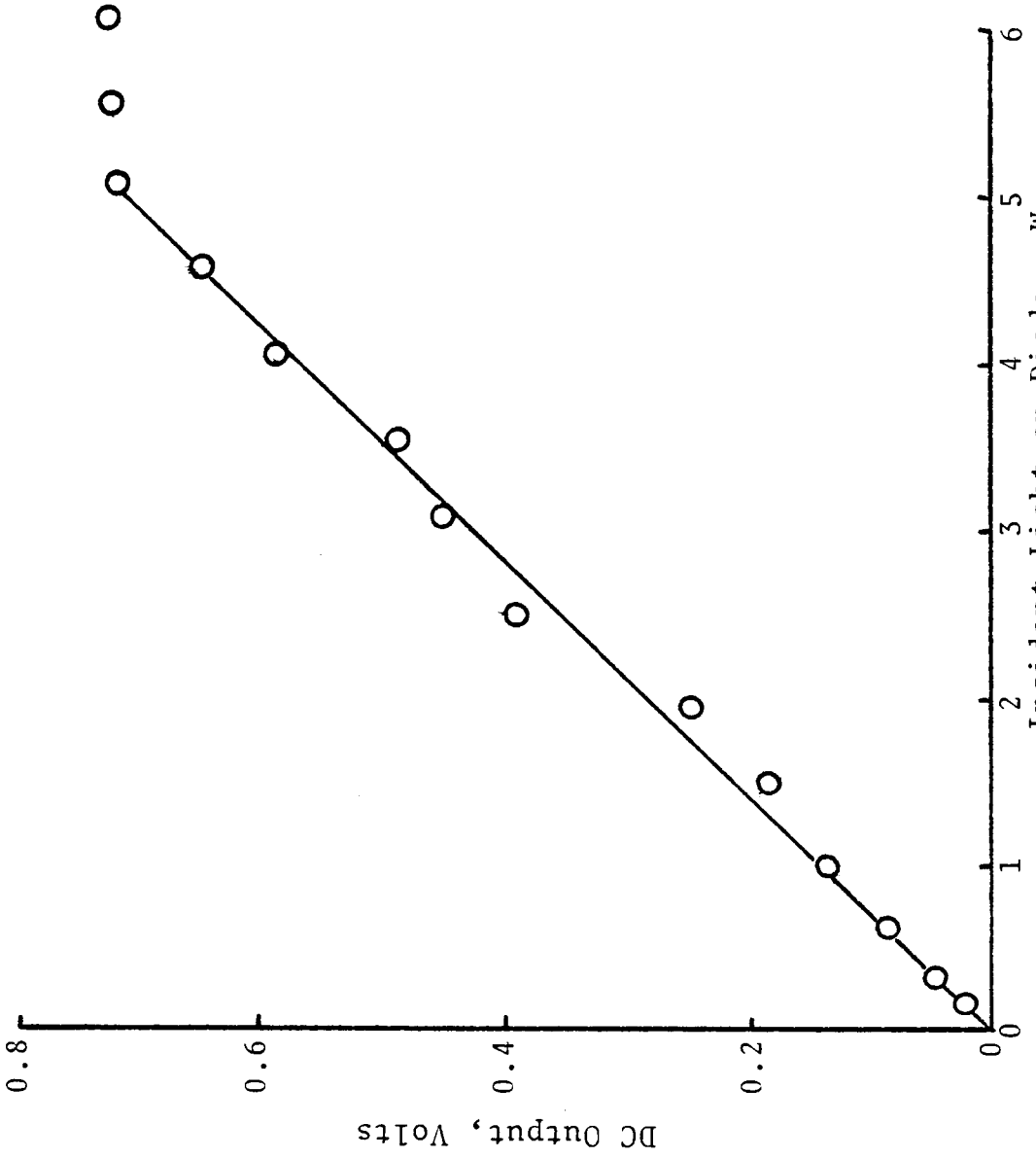


Figure 8. DC Output versus Incident Irradiance.

responsivity agreed within 10% of the manufacturer's given value of 178,000 (V/W), or for a 4,052-Ω resistance, 44 (A/W). The plotted data had a linear correlation coefficient of 0.986.

Aperture Measurements of Visibility and Signal-to-Noise Ratio

In measuring the visibility against the number of spots, the small size and irregular shape of the speckles made it difficult to measure exactly the number of cells within a pattern at the detector plane. It was assumed that the number of spots within an apertured region of the pattern is proportional to the aperture area.

To control the speckle pattern area, an iris diaphragm was inserted behind the beamsplitter just in front of the focusing lens L_2. The reference beam and speckle pattern combination at this point having a radius r_b, is masked down by the iris to a smaller radius r_i. By observing the pattern on a screen in the detector plane, the number of spots in the pattern was seen to be regulated by adjusting the iris. The aperture can also be thought of as controlling the image area of the surface corresponding to the detector seeing fewer scatterers on the tape.

The collecting lens L_1 and the focusing lens L_2 act as an imaging system for directing the light from the surface to the detector. Refer to Figure 9 for the optical configuration. The analysis concerning geometric imaging regards the light cylinder between the two lenses to be well collimated due to the laser beam directionality, surface retroreflectivity, and object-image plane location near the focal planes of the lenses. Although the tape on the surface randomly scatters the light phasewise, the tape has enough retroreflective property to direct the light back along its incident path, providing a beam containing the speckle pattern. This beam traveling to the detector defines distinctly the rays contributing to the image or pattern. The beam is small relative to the lenses and is completely received so that no lens periphery effects are considered.

As the beam reaches the iris, the iris acts as a field stop to limit the size of the image arriving at the detector. If the beads on the surface are considered objects, the iris controls the number of objects in the field of view and, therefore, what is seen by the detector. It is furthermore possible from the geometry and lens magnifications to express the image and object area radii in terms of the iris radius r_i. The collecting and focusing lenses have respective focal lengths of 32 cm

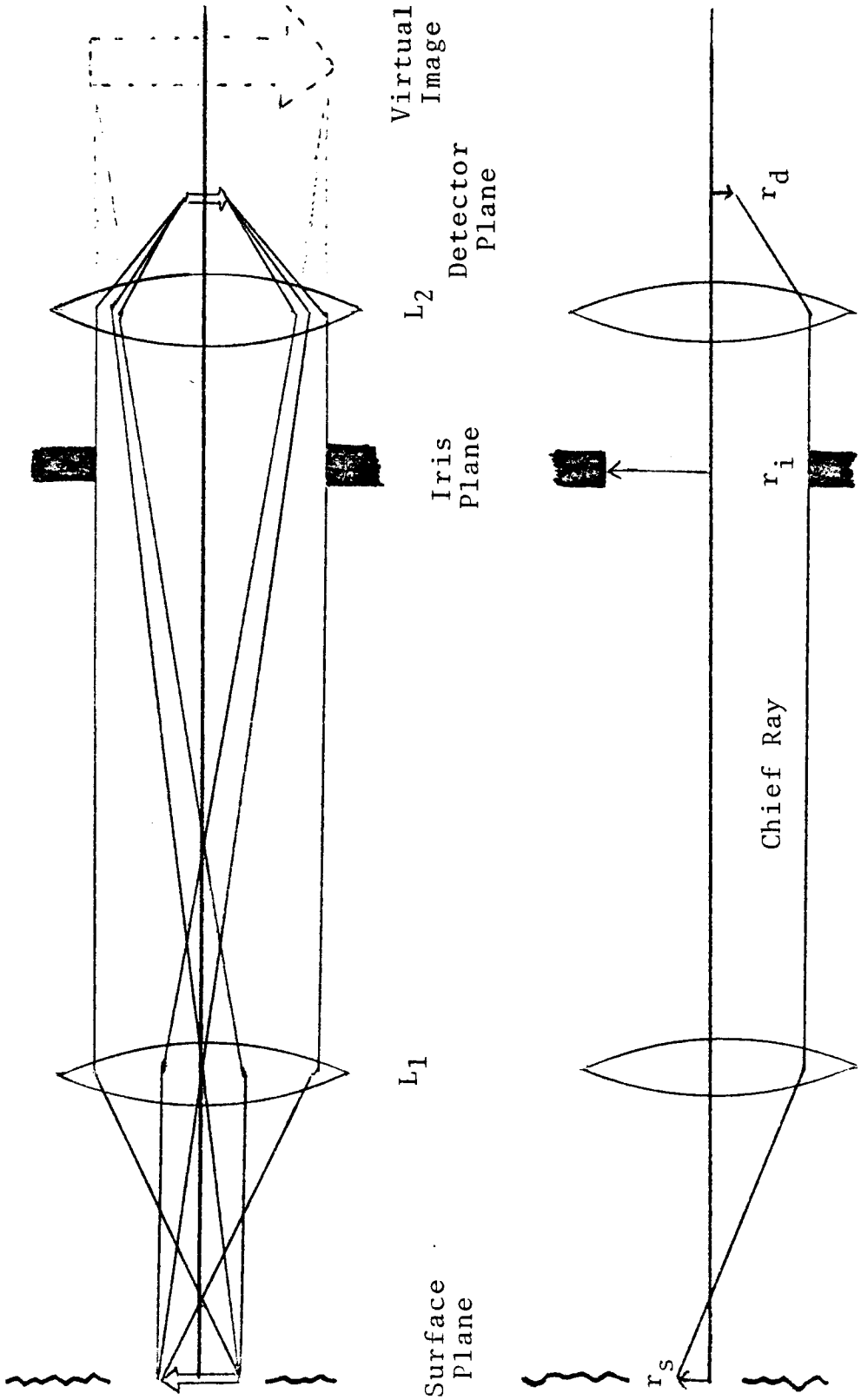


Figure 9. Geometric Optics of Light from Surface to Detector.

and 6 cm and are separated by 71 cm with the detector and surface near the focal planes of each lens. As shown in Figure 9, the image radius on the detector is 1/60 the pattern radius (0.016 r_i), while the object radius on the field of view is 1/12.3 the iris radius (0.081 r_i). This information will allow an approximation of the number of surface scatterers imaged on the detector limited by the diaphragm. Given the size of the scattering beads and assuming they cover uniformly all the area encompassed by the beam, the number of beads in the imaged area is found by dividing the imaged area by the bead area. This results in an approximation of

$$n = \frac{4.13 \times 10^6}{m^2} r_i^2 .$$

For the iris at minimum aperture (r_i=1.1 mm), about five beads are imaged on the detector, while for an unstopped beam $r_i=r_b$, the optics will image perhaps 400. Appendix II explains how these values were calculated.

To increment the diameter of the aperture, a reliable method was needed. The method used involved first measuring the diameter of precision-machined rods with calipers. Then, the iris was closed down on the rod, and the rod was removed. The aperture diameter was assumed to be the same as the rod diameter.

Starting with the largest rod diameter, the diaphragm in front of the detector was stopped down and the detector output voltage was measured on the oscilloscope. The measurement was made by recording the DC output level together with the peak-to-peak amplitude of the AC signal. The diaphragm was successively stopped down to the smallest opening. This procedure was repeated for several different speckle patterns. Using Eq. (14), the visibility values for each aperture size were averaged and plotted in Figure 10. Including the brackets, representing one standard deviation of the values, each average lies on a least squares curve fit proportional to one over the square root of the area. The data show that as the number of spots is reduced, the variance of data points is increased. This is seen by the larger standard deviation brackets. Visibilities from large aperture measures were consistently close to the $1/\sqrt{n}$ point, while small aperture areas had visibilities scattered from higher to lower values. For a few speckles, the potential relative variation in the phase of each spot becomes very significant in affecting the visibility. It is more likely that four or five spots may interfere completely, or not at all, than for the interference of 40 or 50 spots to all contribute constructively or destructively. The resulting

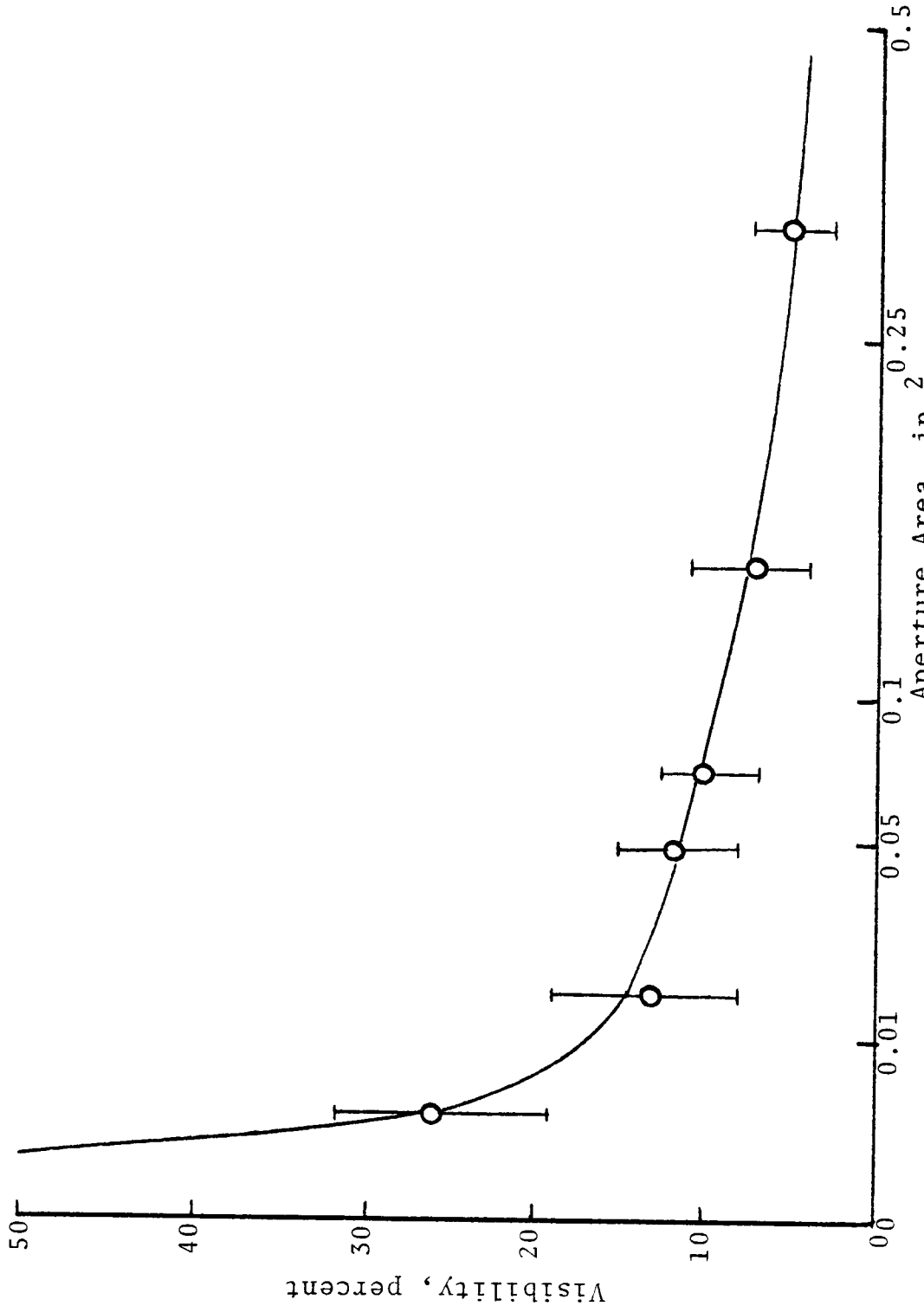


Figure 10. Measured Visibility versus Aperture Area.

visibilities range from very high or low for a few spots to less variant with many spots.

Since the visibility is decreasing with increasing aperture, it would prove informative to calculate the SNR from Eq. (34) for the same measured voltages. The SNR versus aperture is plotted in Figure 11, showing the SNR peaks and then diminishes with increasing apertures. This signal behavior can be explained by diffraction theory [9].

The signal in a heterodyne system can be shown to be a function of a number of Airy rings on the detector [10]. The iris diaphragm, besides acting as a field stop also is a circular aperture that causes diffraction effects that are received at the detector.

The Airy disc field amplitude profile can be written as

$$A_1 = A_o \frac{2J_1(kar/D)}{kar/D} \tag{38}$$

plotted in Figure 12a, where J_1 is the first-order Bessel function, a is the iris source aperture radius, r is the radial variable in the focal plane, D is the source-to-image distance in the focal plane, A_o is the maximum amplitude. If the reference beam has a Gaussian distribution,

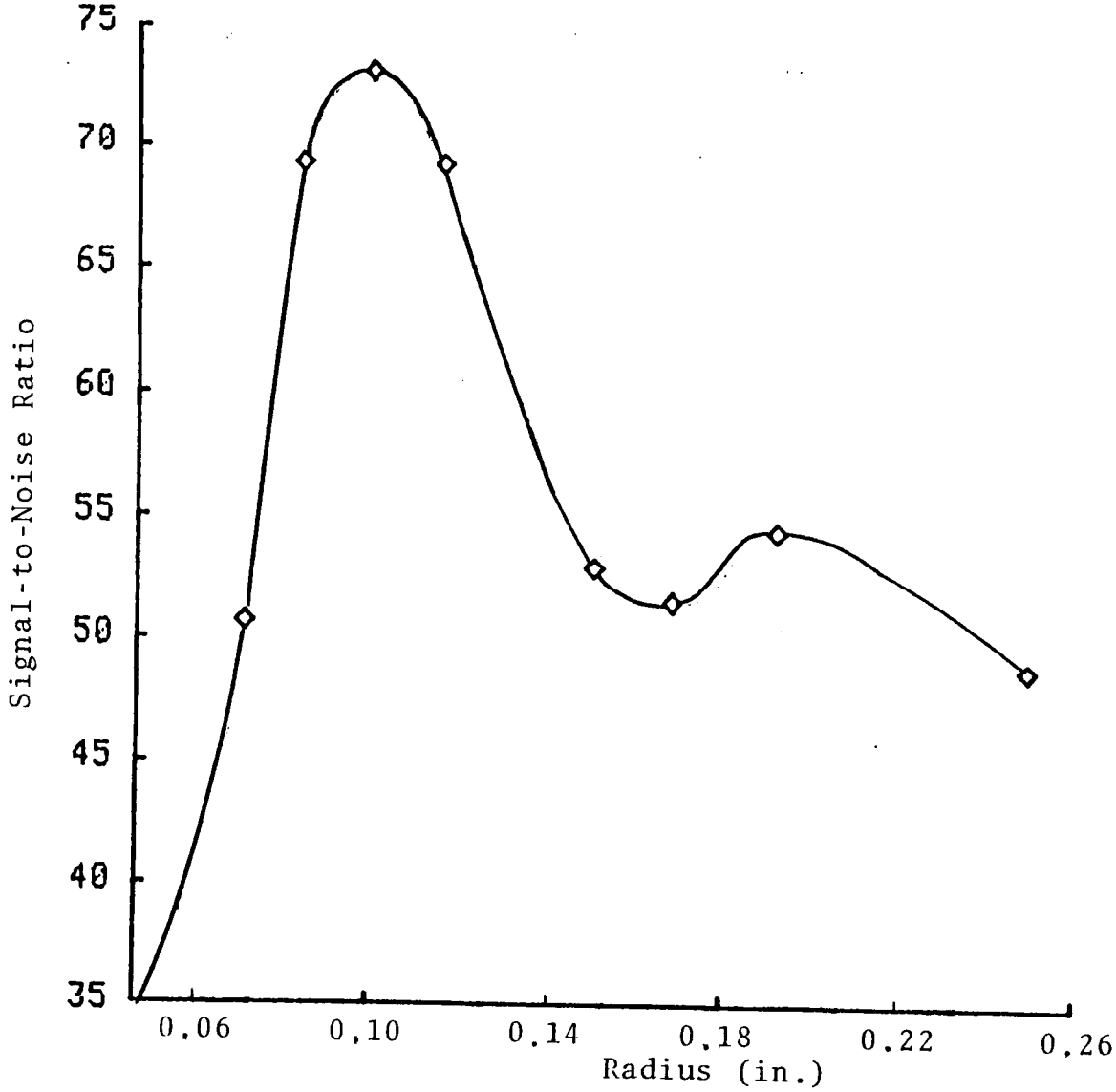
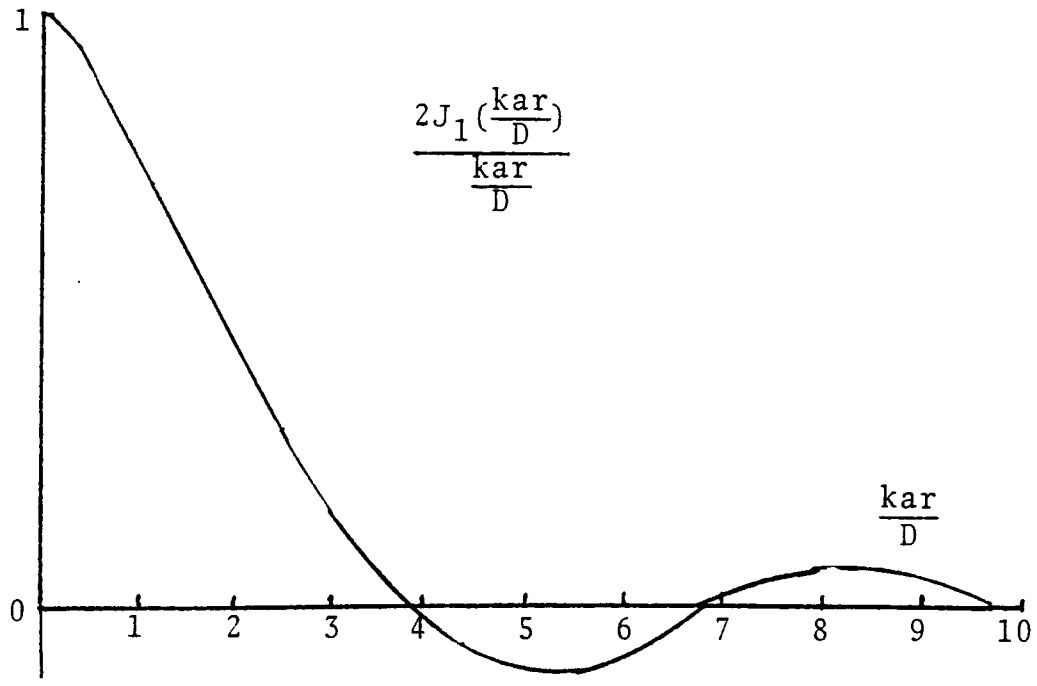
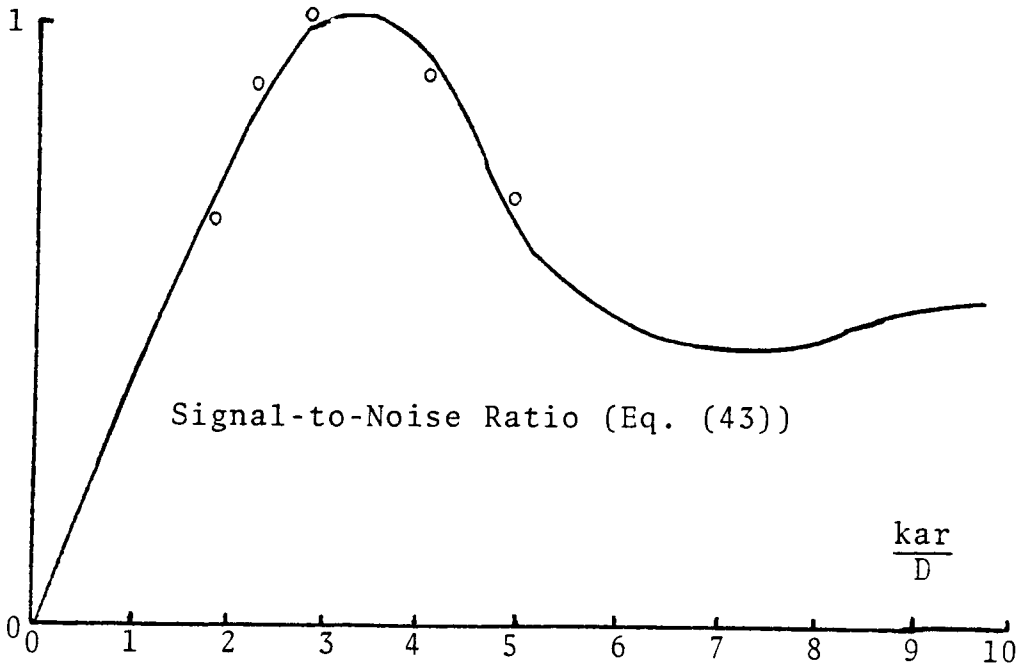


Figure 11. Signal-to-Noise Ratio versus Aperture Diameter.



a. Airy Disc Amplitude versus Radius



b. Normalized Plot of Eq. (43) and Sample Experimental Data

Figure 12. Airy Disc Descriptions of Amplitude, Signal-to-Noise Ratio.

$$A_2 = Re^{-r^2/r_b^2} , \tag{39}$$

with r_b the defined beam radius; then substituting these expressions into Eq. (11) gives the interference equation

$$I = A_o^2\left(\frac{2J_1(kar/D)}{kar/D}\right)^2 + R^2e^{-2r^2/r_b^2} + 2A_oRe^{-r^2/r_b^2}\frac{2J_1(kar/D)}{kar/D}\cos(T) , \tag{40}$$

where T contains all the cosine terms. This expression is the intensity at the focal plane along the radius r of the pattern.

As was shown earlier, the V_{DC} portion of the detector output is given by the $A_1^2+A_2^2$ intensity terms. To correspond to the V_{DC} output, the terms in Eq. (40) are integrated over the detector area to get

$$V_{DC} = \int_{A_T}\left(A_o^2\left(\frac{2J_1(kar/D)}{kar/D}\right)^2 + R^2e^{-2r^2/r_b^2}\right)dA_T . \tag{41}$$

The AC portion will be, likewise

$$V_{AC} = \int_{A_T} 2A_o\frac{2J_1(kar/D)}{kar/D}Re^{-r^2/r_b^2}\,dA_T . \tag{42}$$

In these forms the output voltages of the detector are described in terms of the iris diaphragm area radius.

These expressions can be substituted into the SNR equation (Eq. (34)) to get SNR as a function of radius,

$$SNR = \frac{\int_{A_T} 2A_o \frac{2J_1(kar/D)}{kar/D} Re^{-r^2/r_b^2} dA_T}{\sqrt{N_a^2 + \left(Gz\sqrt{\frac{2eB}{Gz}}\int_{A_T}\left(R^2e^{-2r^2/r_b^2} + A_o^2\left(\frac{2J_1(kar/D)}{kar/D}\right)^2\right)dA_T\right)}} \quad .(43)$$

Equation (43) was solved numerically and plotted in Figure 12b. The curve, like the measured SNR versus radius data in Figure 11, is seen to rise to a peak but then drop off corresponding to the radius at which the second Airy ring is included. This next ring is light that is 180° out of phase from the center spot. The signal V_{AC} depends on the interference of phase terms. Adding these terms that are out of phase relative to the center spot will cause destructive interference and reduce the signal. The V_{DC} and the noise respond only to the amount of light on the detector so that the inclusion of the rings increases the light and, therefore, the noise. So, as the aperture increases to accept more of the Airy pattern on the detector, the signal decreases more and the noise increases. As the iris enlarges to include the third outer ring which has the same phase as the center

spot, the signal will increase again, but not to the level of the first peak. Therefore, to achieve an optimum SNR, the speckle pattern should be stopped down to eliminate the outer noncontributing terms.

Intensity Measurements of Visibility and Signal-to-Noise Ratio

Experimental examination of the relation between visibility and intensity required little modification of the vibrometer. The Bragg cell located immediately in front of the laser provided an adequate way of controlling the light intensity entering the system. Varying the power to the cell altered the amount of light deflected from the main beam.

For the experiment, the light intensity values ranged from just below the diodes' saturation point (600 mV DC output) to the attenuation limit (100 mV DC output) given by the Bragg cell's maximum input voltage. The intensity was adjusted for output increments of 25 mV DC, and the AC level was measured at these points. For each run, different patterns were selected by moving the surface across the beam, which in turn produced different visibilities. A sample run showing the visibility plotted with respect to DC output is in Figure 13.

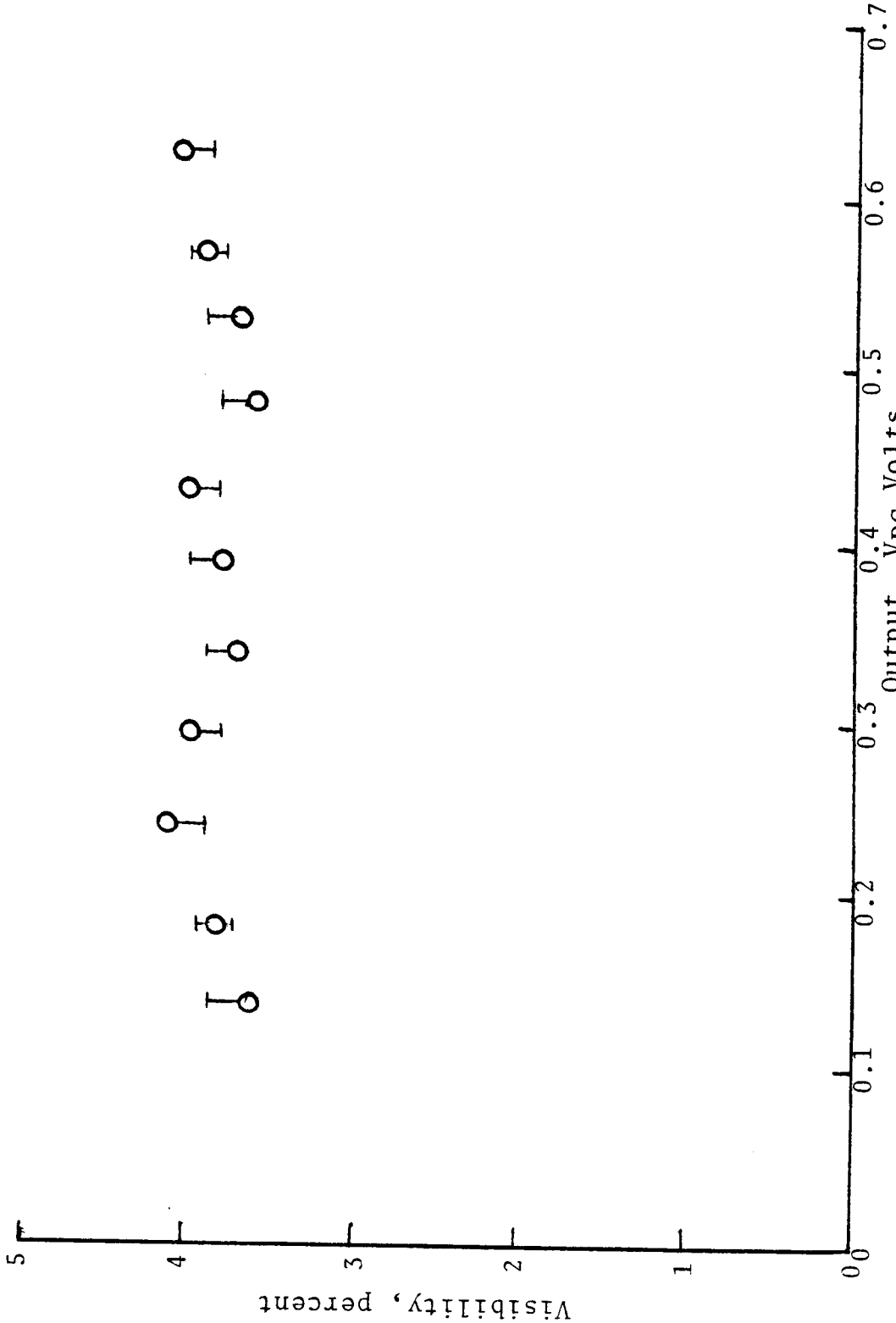


Figure 13. Visibility versus Detector Output.

Over the range of intensities tested for a specific pattern, the visibility values are all within one standard deviation of the mean and do not change.

Using the data from the same run and Eq. (34), the SNR was calculated. Plotted in Figure 14, the data show the SNR increases proportionally to input power as predicted by Eq. (34).

As different speckle patterns were selected for the experiment, notice was given to any appearance of signal dropout. Occasionally, the surface would reflect a pattern with a signal so poor it could barely be read above the noise. Figures 15a and 15b show the signal from a low visibility speckle. However, at higher intensities for the same pattern, the signal begins to improve, as Figure 15a shows over 15b.

Further signal improvement can come with aperture adjustment. Figure 16 shows two typical signals from one fairly high visibility pattern at different intensities. The signals are acceptable, although the higher amplitude waveform in Figure 16b may be preferred. When the aperture in front of the detector stops down the mixed beams to half the arriving image size, the signals sharpen significantly. Applying only the stop, the signal in Figure 17a shows the improvement over the signal in

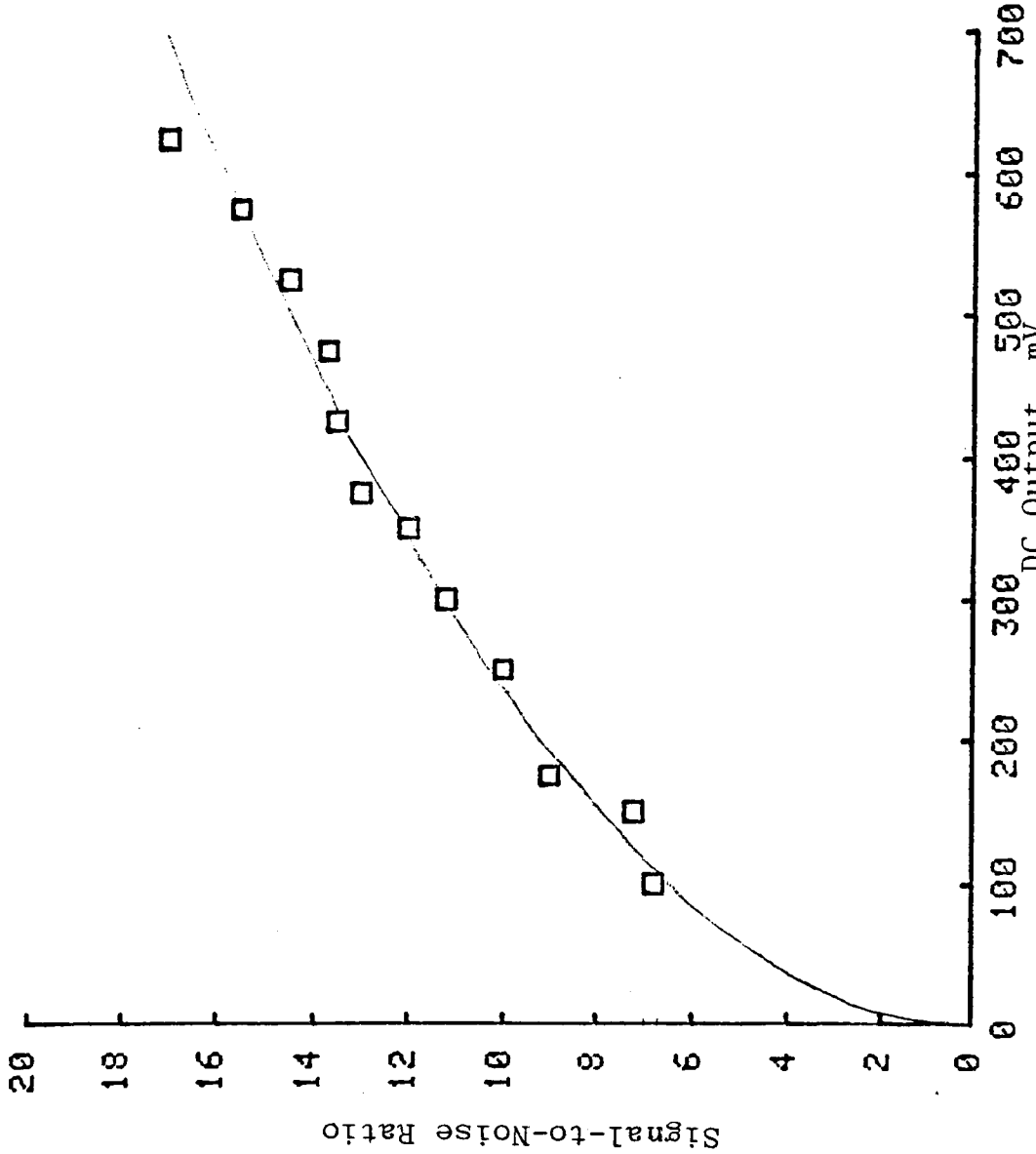
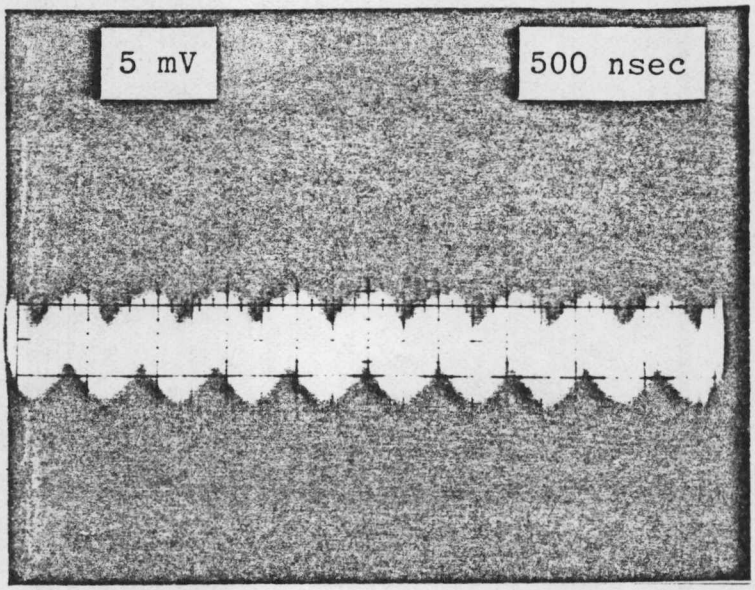
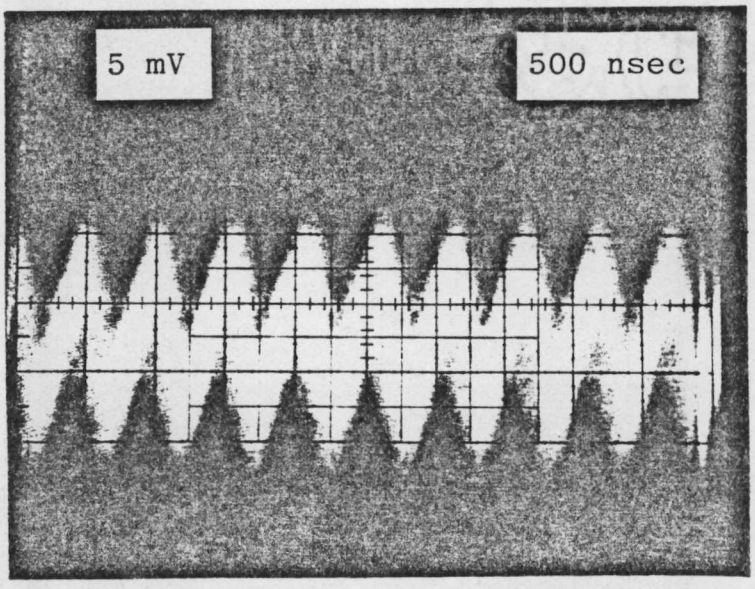


Figure 14. Signal-to-Noise Ratio versus Detector Output.

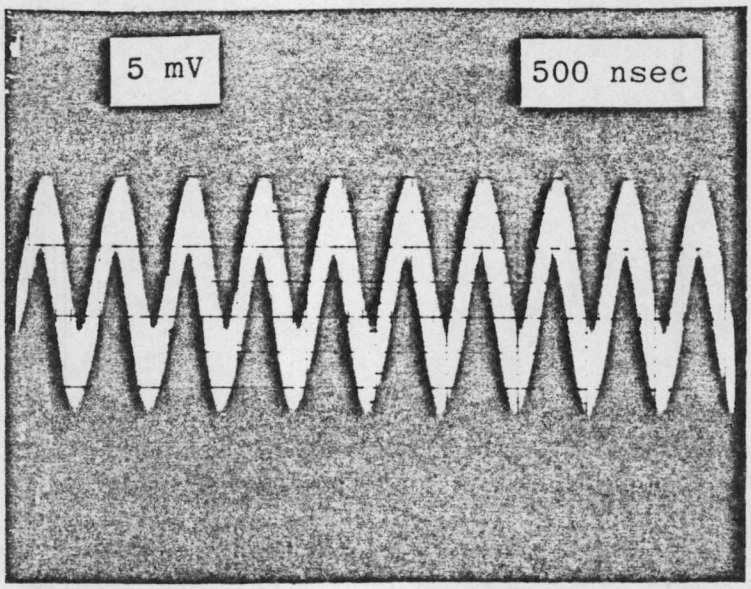


a. Low Intensity, Poor Signal, High Noise

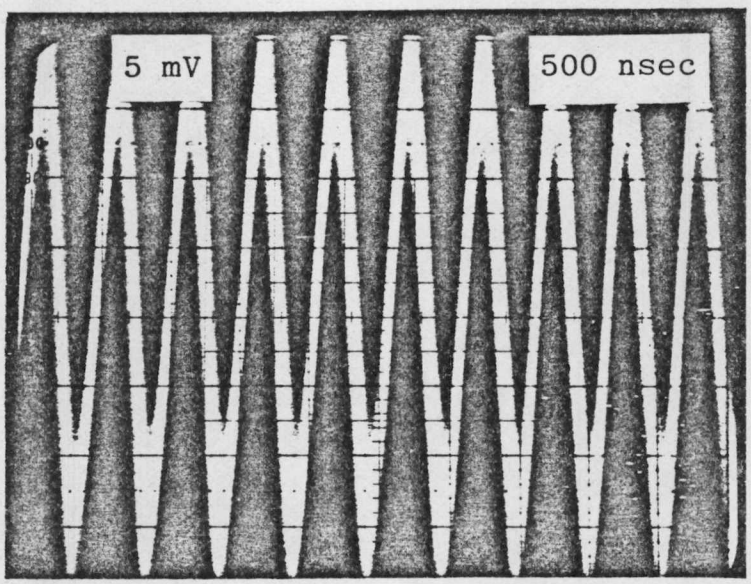


b. High Intensity, Some Improvement

Figure 15. Signals from a Low-Intensity Speckle Pattern.

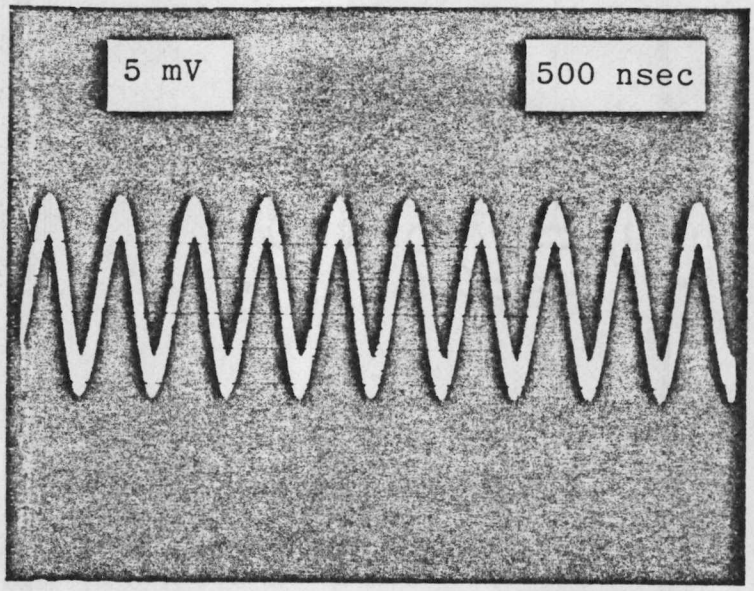


a. Low Intensity

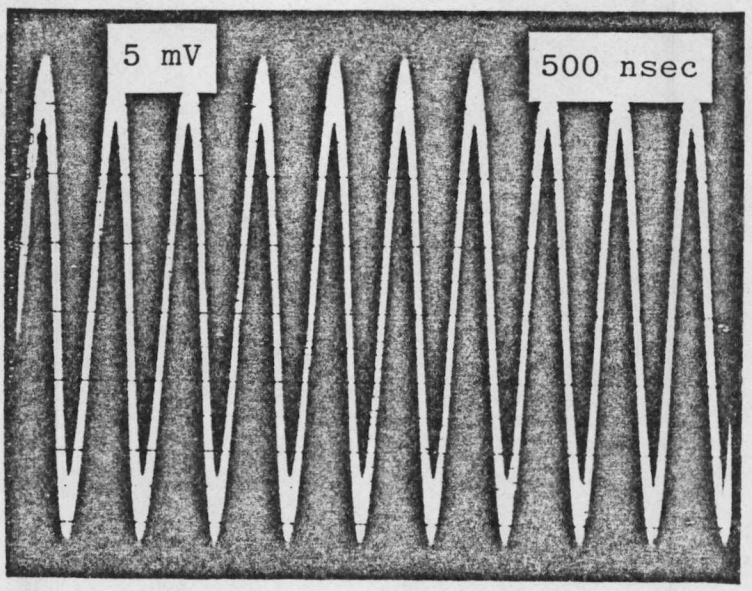


b. High Intensity

Figure 16. Signals from a High-Intensity Speckle Pattern.



a. Low Intensity with Stop



b. High Intensity with Stop

Figure 17. Signals from a Low-Intensity Speckle Pattern with an Aperture Stop.

Figure 16a. Although the visibility of the raw speckle reflection is constant for a stationary surface, the aperture lets the detector see fewer spots and less of the noncontributing beam periphery, thus improving the received visibility.

CHAPTER IV

SUMMARY AND CONCLUSIONS

This paper has studied the laser Doppler vibrometer as a specialized type of interferometer for measuring the direction and displacement of small movements of the target surface. A diffuse surface will scatter the monochromatic laser light with a random phase and generate a speckle pattern at the detector. The heterodyned pattern on the detector from a stationary surface will produce a signal in the output voltage having a certain visibility. The visibility is independent of the laser intensity, as was shown analytically with the mathematical model and experimentally with the instrument. The same model has shown that the visibility varies inversely with the square root of the number of speckle spots received at the detector.

From this study it was shown that there are two ways to improve the signal performance. The light intensity can be increased to just below the saturation point of the diode because a higher incident radiation gives a higher SNR. Secondly, the detector aperture can be stopped down to transmit fewer spots and increase the visibility. The aperture also serves to eliminate the

outer Airy rings which add to the noise. Although the problem of dropout in surface motion measurements persists, these modifications can reduce the severity of its effect.

BIBLIOGRAPHY

BIBLIOGRAPHY

1. Hecht, E., and A. Zajac. Optics. Reading, Massachusetts: Addison-Wesley Publishing Company, 1974.

2. Weltin, Hans. "Light Beats," American Journal of Physics, 30:653, September 1962.

3. Goodman, J. W. "Statistical Properties of Laser Speckle Patterns," Laser Speckle and Related Phenomena, J. C. Dainty, editor. New York: Springer-Verlag, 1975. Pp. 24-36.

4. Forrester, A. T. "On Coherence Properties of Light Waves," American Journal of Physics, 24:192-196, February 1956.

5. Beesley, M. J. Lasers and Their Applications. New York: Halsted Press, 1976.

6. Goldfisher, L. I. "Autocorrelation Function and Power Spectral Density of Laser Produced Speckle Patterns," Journal of Optical Society of America, 55:247-253, March 1965.

7. Pratt, W. K. Laser Communication Systems. New York: John Wiley and Sons, Inc., 1964.

8. Spectra Physics Bulletin No. 3, "Some Demonstration Experiments in Optics Using a Gas Laser." Mountain View, California: Spectra Physics, Inc., 1963.

9. Born, M., and E. Wolf. Principles of Optics. Oxford: Pergamon Press, 1959.

10. Cathey, W. T. "Signal Power in Heterodyne Detection as a Function of the Number of Airy Rings on the Detector," Proceedings of IEEE, 56:93-94, January 1968.

APPENDICES

APPENDIX I

EVALUATION OF EQUATION (21)

It is desired to evaluate

$$I(x,y) = E_R E_R^* + E_{STOT} E_{STOT}^* + 2\,\text{Real}(E_R E_{STOT}^*) \,, \quad (21)$$

where,

$$E_R = Re^{i(2\pi\nu_R t - k_R h)} \quad (19)$$

and

$$E_{STOT} = \sum_{j=1}^{n} \sum_{m=1}^{n} A_1 e^{i(2\pi\nu t - kh + \frac{k}{h}(u_j x + v_m y) + \theta + \phi(u_j, v_m))}. \quad (18)$$

First, the cross terms of $2\,\text{Real}(E_R E_{STOT}^*)$

$$= 2\,\text{Real}\left\{Re^{i(2\pi\nu_r t - k_R h)} \sum_{j=1}^{n} \sum_{m=1}^{n} A_1 e^{-i(2\pi\nu t - kh + \theta + \phi(u_j, v_m) + \frac{k}{h}(u_j x + v_m y))}\right\}$$

$$= 2\,\text{Real}\left\{Re^{i(2\pi\nu_R t - k_R h - 2\pi\nu t + kh - \theta)} \sum_{j=1}^{n} \sum_{m=1}^{n} A_1 e^{-i(\frac{k}{h}(u_j x + v_m y) + \phi(u_j, v_m))}\right\}.$$

Let $\Delta\nu=\nu-\nu_R$ and simplify

$$= 2 \text{ Real } \left\{ Re^{i(2\pi \frac{h}{c} \Delta\nu - 2\pi\Delta\nu t - \theta)} \sum_{j=1}^{n} \sum_{m=1}^{n} A_1 e^{-i(\frac{k}{h}(u_j x + v_m y) + \phi(u_j, v_m))} \right\}$$

$$= 2 \, RA_1 \sum_{j=1}^{n} \sum_{m=1}^{n} \cos(2\pi\Delta\nu(t - \frac{h}{c}) + \theta + \frac{k}{h}(u_j x + v_m y) + \phi(u_j, v_m)) \, .$$

To evaluate the speckle field complement product, simplify the nomenclature by substituting

$$C = \frac{k}{h}(u_j x + v_m y) + \phi(u_j, v_m) \quad T = 2\pi\nu t \quad \text{and} \quad F = \theta - kh \, ,$$

so that Eq. (19) is written

$$E_{STOT} = \sum_{j=1}^{n} \sum_{m=1}^{n} A_1 e^{i(C+T+F)} \, .$$

Then,

$$E_{STOT} E_{STOT}^* = e^{i(T+F)} \sum_{j=1}^{n} \sum_{m=1}^{n} A_1 e^{iC} \, e^{-i(T+F)} \sum_{j=1}^{n} \sum_{m=1}^{n} A_1 e^{-iC}$$

$$= \left[A_1 \sum_{j=1}^{n} \sum_{m=1}^{n} (\cos C + i \sin C) \right] \left[A_1 \sum_{j=1}^{n} \sum_{m=1}^{n} (\cos C - i \sin C) \right]$$

$$= \left[A_1 \sum_{j=1}^{n} \sum_{m=1}^{n} \cos C \right]^2 + \left[A_1 \sum_{j=1}^{n} \sum_{m=1}^{n} \sin C \right]^2 \, .$$

Resubstituting in for C gives

$$= \left[A_1 \sum_{j=1}^{n} \sum_{m=1}^{n} \cos\left(\frac{k}{h}(u_j x + v_m y) + \phi(u_j, v_m)\right)\right]^2$$

$$+ \left[A_1 \sum_{j=1}^{n} \sum_{m=1}^{n} \sin\left(\frac{k}{h}(u_j x + v_m y) + \phi(u_j, v_m)\right)\right]^2 .$$

Finally, the reference beam term is just

$$E_R E_R^* = Re^{i(2\pi\nu_R t - k_R h)} Re^{-i(2\pi\nu_R t - k_R h)} = R^2 .$$

So, collecting all the terms, Eq. (21) is now expressed as

$$I(x,y) = R^2 + \left[A_1 \sum_{j=1}^{n} \sum_{m=1}^{n} \cos\left(\frac{k}{h}(u_j x + v_m y) + \phi(u_j, v_m)\right)\right]^2$$

$$+ \left[A_1 \sum_{j=1}^{n} \sum_{m=1}^{n} \sin\left(\frac{k}{h}(u_j x + v_m y) + \phi(u_j, v_m)\right)\right]^2$$

$$+ 2RA_1 \sum_{j=1}^{n} \sum_{m=1}^{n} \cos\left(2\pi\Delta\nu\left(t - \frac{h}{c}\right) + \theta + \frac{k}{h}(u_j x + v_m y) + \phi(u_j, v_m)\right) . \quad (22)$$

APPENDIX II

COMPUTATION OF IMAGE AND OBJECT RADII

As seen in Figure 9b, page 37, and from simple geometry, it is possible to determine the relationship between the iris diaphragm radius and the image radius at the detector. Assuming the cylindrical beam of light in the iris converges in a cone to the focal point of the lens, then the ratio of the beam diameter to the focal length of L_2 is the same as the ratio of the height of a segment from the axis to the cone and the segment's distance from the focal point. If the detector and the image radius r_c is at x=1 mm from the focus, f_2, the relation is

$$\frac{x}{r_c} = \frac{f_2}{r_i} .$$

For f_2=60 mm, then solving yields

$$r_c = \frac{r_i}{60} .$$

Using the same geometrical assumptions and Figure 9, the surface object area radius r_s that is 2.6 cm in front of the focal point of L_1 (f_1=32 cm) can be expressed

$$r_s = \frac{r_i}{12.3} .$$

Given the size of the scattering beads of $r_{bead} = 40$ μm and assuming they cover uniformly all the area encompassed by r_s, the number of beads in the imaged area is

$$n = \frac{r_s^2}{r_{bead}^2} = \frac{\left(\frac{r_i}{12.3}\right)^2}{r_{bead}^2} .$$

Inserting the value of r_{bead} and simplifying gives

$$n = 4.13 \times 10^6 \ (m^{-2}) \ r_i^2 ,$$

which is the number of beads imaged in terms of the iris diaphragm radius and a constant.

VITA

Vinson B. Huegele was born in Shreveport, Louisiana, on October 4, 1955. As the son of an Air Force pilot, Huegele developed an interest in model aircraft and rockets early in life. He concentrated on science and mathematics courses at W. P. Davidson High School in Mobile, Alabama, from which he graduated in 1973. Later he enrolled in David Lipscomb College in Nashville, Tennessee, and received his Bachelor of Science degree in Physics in 1978. Upon graduation he entered the University of Tennessee Space Institute in Tullahoma, Tennessee, as a Graduate Research Assistant. In 1984 he was awarded the Master of Science degree in the field of Engineering Science.

Mr. Huegele is presently employed as an optical engineer at the National Aeronautics and Space Administration (NASA), Marshall Space Flight Center, Huntsville, Alabama. He is married to the former Sharal Bobo.